University of Turin

Department of Medical Sciences

Ph. D Program in Medical Physiopathology

XXXVI cycle

Development of a novel cellular model to understand genotype-phenotype correlations for Polycystic Kidney Disease patients exploiting CRISPR/Cas9

Supervisor

Professor Silvia Deaglio

Candidate

Martina Migliorero

Coordinators:

Professor Franco Veglio

Professor Benedetta Bussolati

Academic years: 2020-2023

Scientific-Disciplinary Sector: MED/03

Table of contents

Abstract

Autosomal Dominant Polycystic Kidney Disease (ADPKD) is the most common single-gene disorder leading to kidney failure. Almost 80% of cases of ADPKD are attributed to germline variants in *PKD1*, a significant proportion of which is classified as “variant of unknown significance” (VUS). Therefore, a proper experimental model to study the functional impact of different genetic lesions is needed to confirm their pathogenicity.

The aim of my work was to obtain the proof-of-principle of the validity of a cellular model to rapidly generate and functionally test specific *PDK1* variants. To do so, HEK293T cells were transfected with a sgRNA targeting exon 15 of *PKD1* to generate homozygous ($Ex15^{-/-}$) or heterozygous mutants ($Ex15^{+/-}$). The progression of ADPKD is in line with a “double hit” model, which means that inactivation of both copies of *PKD1* by germline and somatic variants is necessary for cyst development. For this reason, *PKD1* WT and heterozygous clones were then used to introduce a specific additional variant, c.11614G>A p.(E3872K), using a cytosine base editor (CBE).

Once confirmed that the expression of Polycystin-1 (PC-1) was consistent with the genetics of the generated cellular lines, we performed RNA sequencing showing that $Ex15^{-/-}$ and $Ex15^{+/-}/Ex42^{M/M}$ clones presented an overall similar transcriptional profile, implying that the missense variant – combined with a more deleterious one – drives the pathological phenotype. GO terms analyses highlighted a dysregulation of ADPKD-related processes, such as cell-adhesion, cell-cycle, cytoskeleton organization and autophagy. Based on RNA sequencing results and previously published literature, functional assays focused on cell-cycle, focal-adhesion formation, apoptosis and autophagic flux were subsequently performed to validate the model and to confirm the pathogenicity of the exon 42 variant, in combination with the exon 15 nonsense variant.

In conclusion, the results presented in this thesis confirmed the feasibility of the model, which will be used to reproduce additional variants of unknown significance identified in *PKD1* gene in our cohort of patients.

Introduction

Autosomal Dominant Polycystic Kidney Disease

ADPKD is a multisystemic disorder characterized by the growth of numerous kidney cysts and increase in kidney volume, eventually leading to End Stage Renal Disease (ESRD) in most patients[1]. Estimating the prevalence of ADPKD has been challenging due to variable age-dependent penetrance and incomplete clinical ascertainment in the general population - alongside with the high genetic heterogeneity - but a recent study based on genomic sequencing of large populations yielded a minimal estimate of 1 per 1,000 livebirths[2]. Genetic studies from patients and animal models have provided hints in disease pathobiology and strongly support a "threshold model" in which cyst formation is triggered by reduced functional polycystin dosage below a critical threshold within individual tubular epithelial cells. Germline and somatic variants in *PKD1* (OMIM #601313) and/or in *PKD2* (OMIM #173910*)* are the foremost cause of ADPKD, with *PKD1* being the most frequently mutated gene. Variants have been less frequently identified also in genes as *SEC63* (OMIM #608648*)*, *SEC61B* (OMIM #609214*), GANAB* (OMIM #104160*), PRKCSH* (OMIM #177060*), DNAJB11* (OMIM #611341*), ALG8* (OMIM #608103), and *ALG9* (OMIM #606941). The disease is characterized by the progressive development of renal cysts that induce proliferation of tubular epithelium causing anomalies in ciliary complexes that eventually end up in excessive fluids secretion. The uncontrolled outgrowth of the cysts leads to a chronic inflammatory process and to fibrosis until the establishment of kidney failure that in about 50% of the patients develops into ESRD by the age of 60. This pathological process culminates with both renal and extra-renal symptoms with frequent detrimental systemic outcomes. Hypertension, gross hematuria, cyst rupture and infection, kidney stones, and flank pain are common kidney complications[3]. Among the extra-renal manifestations, liver and pancreatic cysts, vascular aneurysms, cardiac valve abnormalities, hernias, and diverticulosis are the most frequent[3,4] The prevalence of liver cysts (rare in pediatric patients) increases with age and occasionally are converted into a serious polycystic liver disease (PLD).

ADPKD diagnosis is generally based on the clinical evaluation of the patient and imaging data. Nonetheless, the high heterogeneity of clinical manifestations observed among different individuals makes ADPKD more challenging to diagnose in certain cases. For these reasons, genetic testing became fundamental for those situations where renal ultrasound is not exhaustive (such as atypical PKD), in absence of family history, for patients' relatives

and in prenatal diagnosis. Recently, certain genetic parameters which can help predict the decline of renal function over time and thus the progression of the disease have been determined. For instance, the type of gene involved and the effect of the allelic variant may provide prognostic indications: as an example, protein truncating variants in *PKD1* gene are associated with more rapidly progressive disease and - in some cases - with a very early onset of ADPKD[5,6,7].

ADPKD genetics

In 80-85% of cases, ADPKD is caused by pathogenic variants in *PKD1* gene, while the remaining 10-15% of patients showed alterations in *PKD2* gene. A small percentage of cases between 0.1-0.3% is attributed to pathogenic variants in *GANAB*[8] and *DNAJB11*[9], respectively. However, in a small percentage of patients no genetic cause has been identified. 97% of the diagnosed patients carry single-nucleotide (SNV) or small indels detected by sequencing analysis while about 2-3% of cases are due to the presence of copy number variants (CNVs) detected by multiplex ligation probe amplification (MLPA)[10]. Variants in the *GANAB* gene cause a "milder" phenotype, generally without renal failure but frequently associated to liver cysts. In fact, some individuals are clinically defined as phenocopy of patients with autosomal dominant PLD, characterized by severe polycystic liver disease and few renal cysts[11]. In patients with variants in the *DNAJB11* gene, small bilateral renal cysts are present, generally not related to the increase in kidneys volume, which instead become fibrotic later in life associated with onset of Chronic Renal Insufficiency (CRI) and ESRD between 59 - 89 years (documented in few individuals). The presence of CRI associated with absence of kidneys enlargement is a clinical feature shared with autosomal dominant tubulointerstitial kidney disease (ADTKD) which must be differentiated from ADPKD[6,9].

Among the listed genes, *PKD1* and *PKD2* are characterized by a high degree of allelic heterogeneity estimating a total number of 2,322 different variants in *PKD1* and 278 variants in *PKD2* annotated in the most comprehensive mutational database (relative to ADPKD) in Mayo Clinic[12]. In addition, most of the variants are unique to a single pedigree. Referring to the *PKD1* gene variants annotated in the Mayo Clinic database, 1,225 variants (52.7%) are classified as pathogenic and likely pathogenic: 21.5% nonsense, 22.6% missense, 46.3% large deletions/indels in frames and frameshifts, and 9.6% splicing variants. For *PKD2,* a large proportion of genetic alterations is represented by indel frameshifts (44.9%) followed by nonsense variants (20.7%) while missense and splicing variants account for one third

(33.7%). When considering the family history, it must be noted that almost 10-15% of patients are negative because ADPKD is caused by *de novo* variants, mosaicism or because no medical history concerning patient's relatives is available.

PKD1 and *PKD2* genes and the polycystin complex

PKD1, located on chromosome 16p13.3 consists of 46 exons spanning 52 kb of genomic DNA characterized by regions enriched in GC (62.4%)[13]. It encodes for polycystin-1, a large membrane protein of 4302 amino acids. The 3' end of the gene partially overlaps with the 3' end of the *TSC2* gene (OMIM #191092) in a "tail-to-tail" orientation. Contiguous deletions removing the tails of both *PKD1* and *TSC2* genes cause a more severe form of PKD which is generally infantile[14,15]. The complexity of *PKD1* relies on the fact that the region between the 5' of the gene and exon 33 turns out to be duplicated in six pseudogenes that map proximally on chromosome 16. These six pseudogenes share 98% sequence homology in the exonic regions[16].

PKD2, located on chromosome 4q21-23, consists of 15 exons encoding for polycystin 2 (PC-2), a 968 amino acids protein.

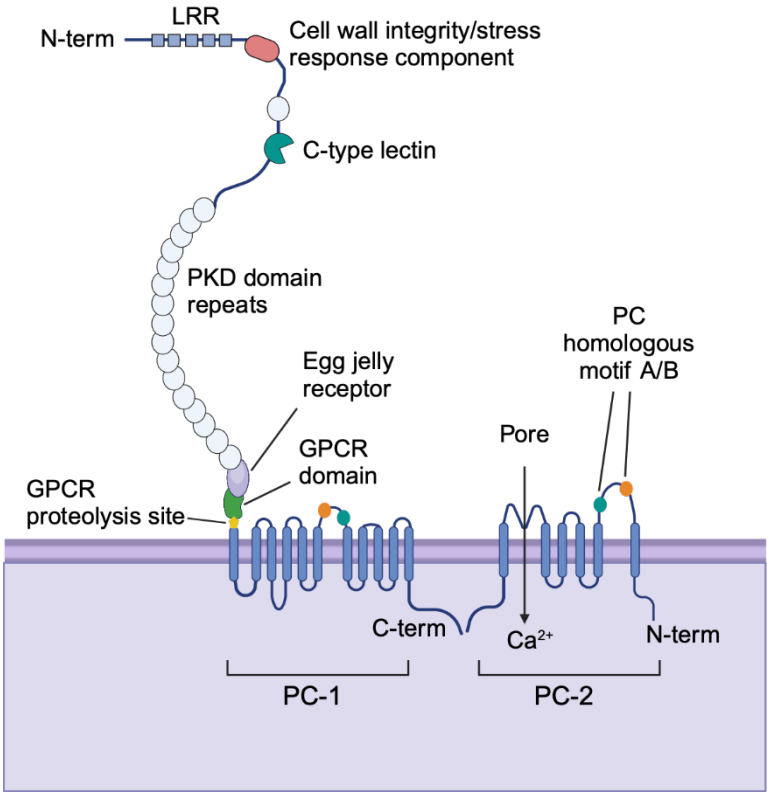

Figure I. The PC-complex. Structure of Autosomal Dominant Polycystic Kidney Disease's proteins, PC-1 and PC-2, structurally and functionally coupled in the so-called PC complex[17]. Image created with Biorender.

PC-1 is composed of a long extracellular N-terminal portion, 11 transmembrane domains, and a short intracellular C-terminal portion (**Figure I**). The extracellular portion comprises different domains, including i) two cysteine-flanked leucine-rich repeats (LRR) domains, capable of binding collagen, fibronectin, and laminin of the extracellular matrix; ii) a cell-wall integrity and stress-response component (WSC) homology domain suggesting that the protein is able to bind carbohydrates; iii) the first of 16 IgG-like repeats (also known as PKD repeats), which bind receptor protein tyrosine phosphatases; iv) a C-type lectin domain that binds carbohydrate in a calcium-dependent manner; v) 15 additional PKD repeats with surface β-pleated folds and the ability to bind protein ligand; vi) a receptor for egg jelly (REJ) homology domain and vii) a latrophilin (CL-1–like GPS) domain which could be a protein-cleavage site. The 200-amino-acid intracellular C-terminal tail contains several protein-interaction and phosphorylation-signaling sites, as well as specific tyrosine sites that can be phosphorylated by c-src and focal adhesion kinase (FAK) and serine phosphorylation sites, targets of protein kinase A (PKA)[18].

PC-2 is composed of six transmembrane domains with a pore homology region in the extracellular loop between transmembrane domains (TM) 5 and 6 and the intracellular N- and C-terminal domains. The C-terminal contains a coiled-coil domain, called CT1 and CT2[18]. CT1 recognizes and binds PC-1 C-terminal domain, whilst CT2 is responsible for the oligomerization between multiple PC-2 proteins to form oligomeric complexes.

Several studies suggest that PC-1 and PC-2 form a heterocomplex with a 1:3 stoichiometry. Indeed, the cryo-EM structure of a PC-1/PC-2 heteromer reveals that the 11 transmembrane helices of PC-1 are further divided into two major domains: a peripheral TM1-TM5 complex and a core TM6-TM11 complex that interlinks with three PC-2 subunits to form a TRP-like ion channel[19].

Kotdaji Ha al.[20] demonstrated that PC-1/PC-2 heteromeric complexes exhibit distinct biophysical properties and that PC-1 members are critical for adjusting the electrical excitability of primary cilia in response to the local environment. By expressing membrane-targeted PC-1 with PC-2 in mammalian cells, they showed that the PC-1 N-terminus is essential for the activation of complexes containing PC-2 subunits. Specifically, the PC-1 C-type lectin domain within the N-terminus, which is a crucial hotspot for ADPKD-causing variants[21], seems to play a key role in channel activation and is believed to interact with the tetragonal opening for polycystins (TOP) domain of PC-2. Both PC-1 and PC-2 have a large extracellular TOP domain, which contain prominent glycosylation sites. The C-type lectin domain in the native PC-1/PC-2 complex likely interacts with glycans in the TOP domain, which allosterically regulates the ion permeation pathway and/or gating apparatus of the heteromeric polycystin channel[22].

Genotype-phenotype correlation and complex inheritance models

ADPKD is classically inherited as an autosomal dominant disease, but recent advances in the field of molecular genetics underlined that the pattern of inheritance is far more complex. For instance, the existence of hypomorphic or not fully penetrant alleles, the presence of variants in other genes responsible for cystic kidney disease or unidentified modifier genes, as well as the influence of environmental factors (i.e., acute kidney injury may influence cyst formation and disease progression[23]) all contribute to make the pattern of inheritance more complicated. According to the gene dosage model, the probability of cyst occurrence increases when the level of functioning PC-1 protein falls below a critical threshold; consequently, the type of variants affects the probability of cyst formation and the disease progression[17] (**Figure II**).

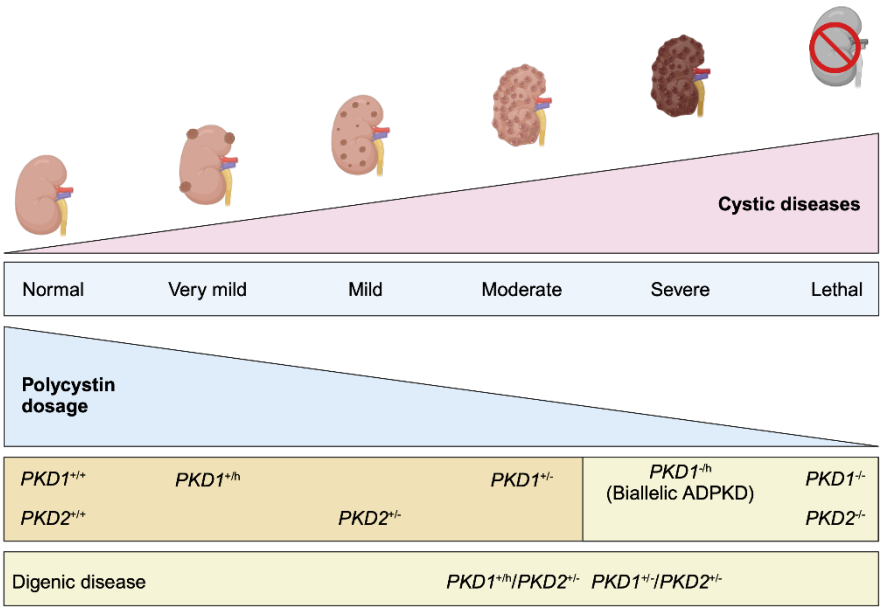

Figure II. The dosage model of cystogenesis in autosomal dominant polycystic kidney disease. The level of functional polycystin 1 directly influences the renal phenotype in patients with autosomal dominant polycystic kidney disease (ADPKD). Image created with Biorender.

Subjects with truncating variants in the *PKD1* gene generally have larger total kidney volume (TKV) compared with subjects with non-truncating variants who end up in this stage by the age of 70 years old (**Figure III**). However, Hwang et al.[24] showed that the renal disease severity in the latter class of mutations is heterogeneous: *PKD1* non truncating variants are classified in two distinct categories, the non-conservative variants in well conserved sites and the conservative variants in not conserved sites. The first ones present a similar outcome as *PKD1* truncating variants in terms of estimated Glomerular Filtration Rate (eGFR) and TKV[7]. On the contrary, the non-conservative variants are classified as hypomorphic, meaning that they are not fully penetrant[25] and need a second variant on *PKD1*/*PKD2* to be phenotypically effective. Given the high heterogeneity, determining the pathogenicity of non-truncating variants is not always easy[26,27], and predicting their clinical effects could be challenging. In silico bioinformatic prediction and family–based segregation studies can provide additional support to determine the pathogenicity of a putative non truncating variant. Moreover, the presence of other affected family members with sufficient renal function or ESRD after 65 years of age can be taken as evidence that the non-truncating mutation of interest likely functions as a hypomorphic allele. Conversely, the presence of other affected family members with ESRD before 50 years of age suggests that

the non-truncating variant is likely completely inactivating. In the absence of an informative family history, TKV may be used as an alternative indicator for renal disease severity[28]. Similar to variants in *PKD1*, truncating variants in *PKD2* have been found to be associated with more severe disease with lower eGFR values than non-truncating variants[29] but there is no strong evidence to date confirming this correlation. Patients with biallelic variants in *PKD1* or *PKD2* have also been described. Hypomorphic variants in homozygosity may not develop the disease until adulthood or may show early disease onset fallaciously guiding the diagnosis toward autosomal recessive polycystic kidney disease kidney disease (ARPKD) in the absence of familiarity[30] as occurs when there is co-presence *in trans* of an hypomorphic allele with a typical penetrant allele[31]. Finally, only rare cases of ADPKD with neonatal onset have been associated with homozygosity of a hypomorphic *PKD2* allele arising from uniparental disomy[32]. Lastly, individuals carrying pathogenic variants in both *PKD1* and *PKD2*, thus double heterozygotes, have been described in literature (digenic ADPKD and trans-heterozygosity) as patients with a more severe renal disease than that reported in heterozygous relatives[33,34,35]. It is worthy to note that unraveling the complex genetic landscape of ADPKD is essential both for diagnosis and for treatment decision. Indeed, there are several studies associating a differential outcome in patients treated with tolvaptan based on their genetics. Tolvaptan is a vasopressin type 2 receptor antagonist whose function is to alleviate renal cyst growth and preventing eGFR dropping over time. Sekine et al.[36] showed that in their cohort of 18 patients diagnosed with ADPKD, the efficacy of tolvaptan seems to differ between patients with *PKD1*/*PKD2* truncating and non-truncating variants, compared to the ones that do not show any alterations in *PKD1*/*PKD2*. These findings suggest that physicians should consider *PKD1/2* variants when administering tolvaptan as their positive or negative outcome depends on them.

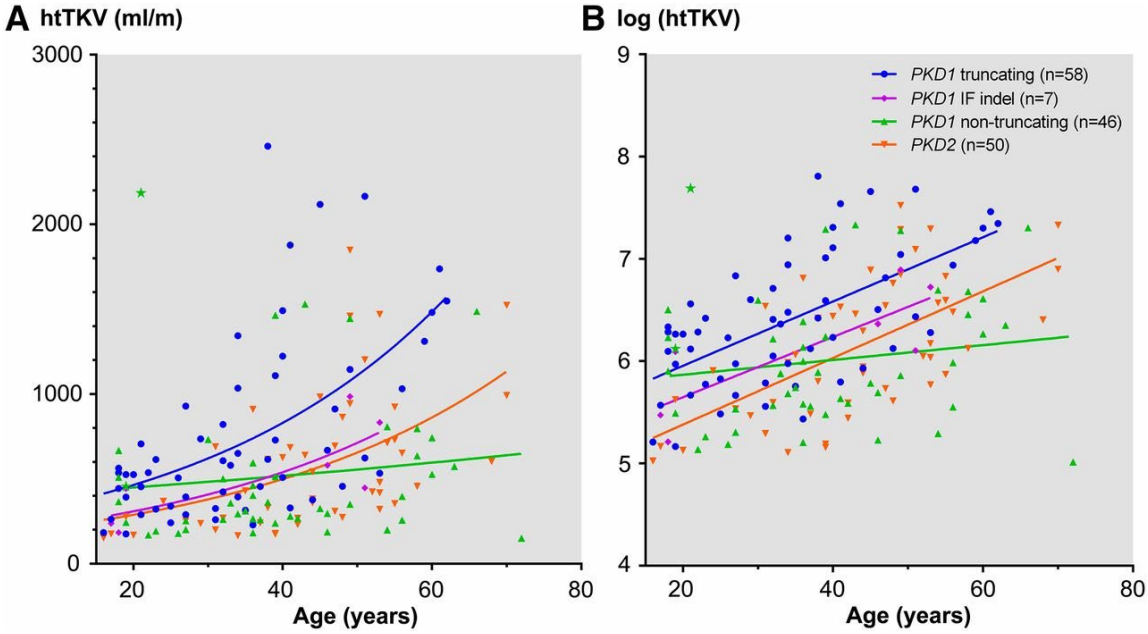

Figure III. Effects of mutation class on htTKV. (A) Corrected for age, patients with *PKD1* protein truncating (PT) mutations generally have larger height adjusted (ht) TKV compared with those from other mutation classes. (B) Assuming exponential growth, the rate of htTKV expansion seems similar between patients with *PKD1* PT, *PKD1* in-frame (IF) indel, and *PKD2* mutations; however, the absolute htTKV (*y* intercept) differs between the three mutation classes. By contrast, the rate of htTKV expansion associated with non-truncating (NT) *PKD1* mutations seem to be significantly slower than the rates of the other three mutation classes. Image taken from[24].

Mechanisms of cystogenesis

Renal cysts are focal outgrowths of the fluid-filled renal epithelium that form mainly at the level of the distal renal tubules and gradually grow due to abnormal cell proliferation, fluid secretion and extracellular matrix production[17].

Formation of cysts occurs prenatally in about 1-3% of nephrons, but they are detected mainly in adults. The most widely accepted theory for cyst formation in human PKD is the “two-hit hypothesis”. Patients with ADPKD are typically heterozygous, with one allele having a germline variant (first hit), whereas the other is normal. In humans, the two-hit hypothesis predicts that the remaining normal *PKD1* allele develops a somatic variant (second hit) in an extremely small percentage of cells. Whole genome sequencing performed on 90 unique kidney cysts obtained during nephrectomy from 24 unrelated participants revealed that pathogenic somatic "second hit" alterations disrupting *PKD1* or *PKD2* were identified in 93% of the cysts. Of these, 77% of cysts acquired short mutations in *PKD1* or *PKD2*; specifically, 60% resulted in protein truncations (nonsense, frameshift, or splice site) and 17% caused non-truncating mutations (missense, in-frame insertions, or deletions)[37]. In some of the

cysts where no homozygous mutation of a PKD gene was found, compound heterozygous variants were identified, suggesting that trans-heterozygosity could be a sufficient condition to induce cyst formation[38].

From a molecular point of view, variants impacting the expression of polycystin affect different intracellular signaling pathways (Ca^{2+}, cAMP, mTOR, WNT, VEGF) causing cellular hyperproliferation and excessive fluid secretion, events that drive cystogenesis. Cyst expansion causes the establishment of a positive feedback loop that continuously increases tissue fibrosis[17]. Indeed, expanding cysts induce mechanical stress in the surrounding tissue and vessels resulting in activation of the repair processes of the cellular damage, causing secretion of inflammatory cytokines and growth factors into the renal tubules and into the surrounding interstitium. Transforming growth factor beta (TGF-β) secretion leads to de-differentiation, recruitment of infiltrating cells to the cyst site and activation of α-Smooth Muscle Actin (αSMA)-positive myofibroblasts with increased extracellular matrix deposition. Pro-inflammatory stimuli and fibrosis accumulation lead to dissociation of pericytes with subsequent rarefaction of the microvasculature and local hypoxia, which exacerbate the fibrosis. Inflammatory cytokines, such as TNF-α, IL-1β and INF-γ activate two major inflammatory pathways in renal epithelial cells: NF-κB and JAK/STAT.

As a result, pro-inflammatory molecules are produced and released, attracting and activating even more infiltrating cells, which aggravate local injury and eventually contribute to cyst progression.

Cell biology

Under physiological circumstances, polycystins are essential for the regulation of the differentiated phenotype of the tubular epithelium. Reducing polycystins expression below a critical threshold triggers a phenotypic transition characterized by the inability to maintain planar polarity, remodeling of the extracellular matrix, high rates of proliferation and apoptosis[39].

Cell-cell contact, cell-matrix interactions, and cytoskeletal rearrangement

Epithelial cells are comprised of two major types of cytoskeletal anchoring junctions: cell-cell junctions localized at the lateral surfaces and cell-matrix junctions localized at the basal surface. Cell-cell junctions include the adherens junctions and desmosomes which link the actin and intermediate filaments, respectively, of adjacent cells. Cell-matrix junctions link these filaments to the extracellular matrix (ECM) and include the actin-linked cell-matrix junctions and focal adhesions

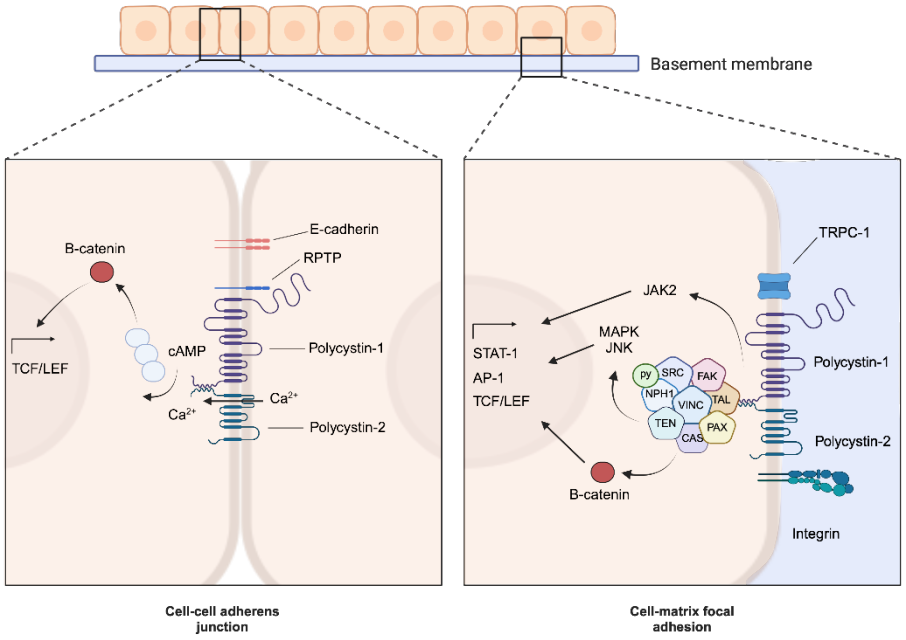

Figure IV. The role of PC-complex in regulating cell-adhesion. Polycystin-1 complexes are found at the cell–matrix interface and cell–cell contacts, where they interact with proteins of the cell membrane, actin and tubulin cytoskeleton and transduce signals by means of intracellular phosphorylation cascades to regulate gene transcription in the nucleus. Image created with Biorender and adapted from[18].

Co-localization and co-immunoprecipitation studies showed that PC-1 forms multiprotein complexes with α2β1-integrin, talin, vinculin, paxillin, p130cas, FAK, β-catenin and E-cadherin in normal human fetal collecting tubules and sub-confluent epithelial cultures[40] (**Figure IV**). In ADPKD epithelial cells, the assembly and stabilization of E-cadherin containing adherens junctions is disrupted[41]. This study suggests that PC-1 may function in the assembly and stabilization of adherens junctions, and variants in *PKD1* may lead to impairment of kidney epithelial cell-cell adhesion. This hypothesis is consistent with the observation that cell adhesion and proper tubule diameter is altered in cystic structures and loss of cell adhesion can trigger cell proliferation, a major hallmark of PKD.

Streets et al.[42] observed that abnormalities in the actin cytoskeleton were a common feature of patient-derived cystic cell lines with variants in *PKD1*. Actin fibers appeared to be thicker, shorter, and more disorganized compared with non-cystic controls. Another interesting finding from the same group is related to cilium structure: indeed, the authors demonstrated that under conditions promoting optimal cilia formation (48-hour serum starvation), the

percentage of ciliated cells as well as cilia length were reduced in cystic cells carrying *PKD1* variants[42].

Another key structure involved in cytoskeletal rearrangement that is altered in ADPKD are the focal adhesions (FA; **Figure V**).

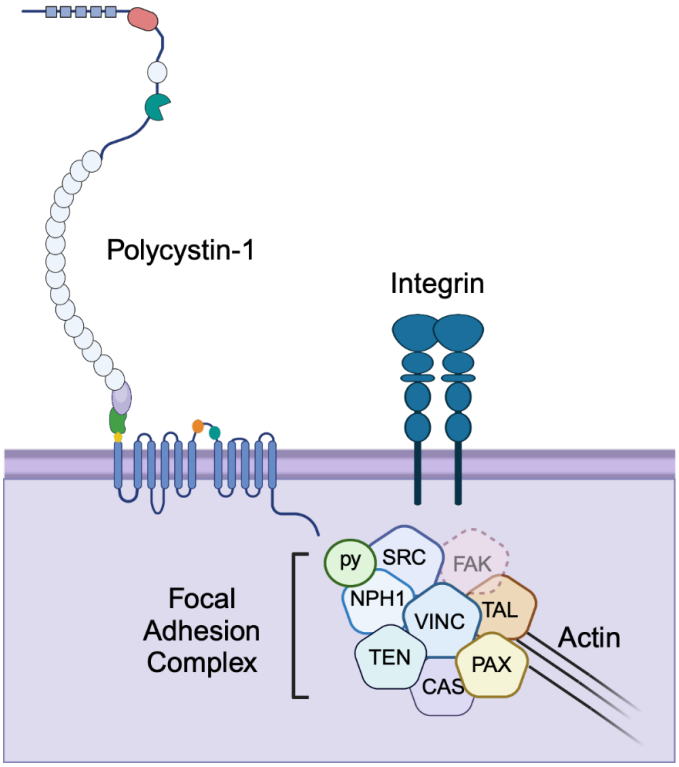

Figure V. Polycystin-1 and Focal Adhesion Complex. In normal renal epithelia, PC-1 interacts in a multiprotein complex with integrins and focal adhesion proteins, including the focal adhesion kinase (FAK). In epithelia from patients with ADPKD, although polycystin-1–focal-adhesion complexes are formed, they lack FAK. TAL stands for talin, PAX paxillin, VINC vinculin, CAS p130-cas, SRC c-src, TEN tensin, and NPH1 nephrocystin. Image created with Biorender.

During renal development the PC complex interacts with FAs and adherens junction proteins to properly guide ureteric bud migration and normal tubule epithelial differentiation[43]. Castelli et al.[44] demonstrated that PC-1, by regulating the activation status of FAK, modulates the stability of the microtubules, as well as the actin cytoskeleton, impacting the turnover rate of FAs in migrating cells. Moreover, overexpression of a PC-1 C-terminal fragment in collecting duct cells stimulated FAK and paxillin phosphorylation, increasing the association between these two proteins and stimulating the formation of focal adhesion complexes[45].

Overall, these studies suggest that PC-1 plays important roles in regulating cytoskeletal dynamics, cellular mechano-sensation and adhesion, all critical biological features for tissue integrity maintenance and prevention of cyst formation in ADPKD.

Apoptosis, proliferation and cell cycle

A precisely controlled balance between cellular proliferation and programmed cell death (apoptosis) is essential for normal growth and differentiation of the kidney and maintenance of normal renal structure after birth. Both these fundamental processes are disturbed in polycystic kidneys. In both ADPKD and ARPKD, apoptosis is abnormally persistent[46] and can be the cause of the alteration of the renal parenchyma, allowing cystic tissue to proliferate. The importance of apoptosis has been highlighted in knockout mice, in which the dual inactivation of inhibitors of apoptosis (*bcl-2* or activating protein 2β [AP-2β]) causes disease manifestation[47,48]. The same process can be appreciated in *in vitro* models such as Madin-Darby Canine Kidney cells (MDCK) cells, where apoptosis is essential for cyst cavitation when cells are grown in a 3D environment. Moreover, in the same system cystogenesis is inhibited by overexpression of the anti-apoptotic gene *bcl-2*[49]. In line with these data, expression of human *PKD1* in MDCK cells slows their growth and protects them from apoptosis[50].

In summary, most *in vitro* and *in vivo* studies in PKD cells support the notion that increased levels of apoptosis are associated with formation and growth of cysts[51]. On the contrary, Carvalhosa et al.[52] demonstrated that $CD133^+$ progenitor cells – representing the cyst-lining cells - derived from ADPKD patients showed a marked resistance to apoptosis induced by serum deprivation compared to normal $CD133^+$ cells. Moreover, treatment with rapamycin was able to revert mTOR activation in PKD $CD133^+$ cells to normal levels and to significantly decrease the proliferation rate, resistance to apoptosis and cystogenesis. These results are in line with experimental data showing that treatment with rapamycin can reduce cyst expansion[53,54,55].

An imbalance between cell proliferation and apoptosis seems to contribute to cyst growth and renal tissue remodeling in ADPKD[56,57]. Moreover, cultured epithelial cells from these patients have an increased intrinsic capacity to proliferate and survive. Li et al[58] demonstrated that PC-2 regulates the cell cycle through direct interaction with Id2, a member of the helix-loop-helix (HLH) protein family that is known to regulate cell proliferation and differentiation. Id2 expression suppresses the induction of a cyclin-dependent kinase inhibitor, p21, by either PC-1 or PC-2. As a result, variants in either *PKD1* or *PKD2* contribute to the abnormal cellular proliferation which is a major hallmark of ADPKD and a trigger for cyst formation. Restoration

of the normal subcellular distribution of Id2 therefore could represent a novel therapeutic strategy for the treatment of ADPKD.

Autophagy

Autophagy is a cellular recycling system that allows the reuse of old and damaged cell parts. Usually, the term autophagy refers to the macro-autophagy, which is a complex process for the lysosomal-dependent degradation of waste cellular material. In response to endogenous or exogenous stimuli, the autophagic activator complex forms a double membrane structure that sequesters the cargo and elongates, producing spherical vesicles (autophagosomes). These vesicles eventually fuse with lysosomes (autolysosomes), where the cytoplasmic material undergoes degradation[59]. Two key kinases regulate the process: the adenosine monophosphate-activated protein kinase (AMPK) and the mammalian target of rapamycin (mTOR). AMPK stimulates autophagy by phosphorylating ULK1, while the mTORC1 complex inhibits autophagy by preventing its activation[53].

Several studies highlighted the dysregulation of autophagy in PKD, demonstrating both increased and decreased autophagy activity across various experimental models. Impaired autophagy can contribute to the accumulation of damaged cellular components and cyst formation, while augmented autophagy may be the cause of a worsening of cyst growth.

PC-1 and PC-2 play crucial roles in the autophagic process. PC-1 regulates calcium-dependent calpain proteases and maintains lysosomal integrity[60], while PC-2 forms a complex with Beclin-1[61]. The interplay between autophagy and apoptosis has been observed in murine PKD models, where suppressed autophagic flux correlates with increased apoptosis, leading to tubular epithelium proliferation and subsequent cyst formation[51]. It has been shown that PC-2 is a critical mediator of autophagy induction[61,62] and that basal autophagy is enhanced in PC-1-deficient cells, meaning that PC-1 promotes autophagic cell survival.

It is also noteworthy that there is a reciprocal interaction between autophagy and primary cilia. It has been shown that signaling from the cilia induced autophagy, while inhibition of autophagy increased cilia growth[63]. In human kidney proximal tubular cells, mTOR activation was enhanced in cilia-suppressed cells and MG132, an inhibitor of the proteasome, could largely reverse autophagy suppression. These findings underline a reciprocal regulatory relationship between cilia and autophagy[64].

The key molecule that links autophagy and cilium signaling is mTOR, which turned out to regulate a critical signaling pathway in cystogenesis [65]. In PKD cells with short cilia, mTOR is activated and autophagy is repressed. Several studies have demonstrated that mTOR

inhibitors can slow down cyst growth, reduce kidney volume and improve its function in rodent models of PKD[66,67,68]. Nevertheless, the findings from these studies are not conclusive. It has been noted that the inhibition of autophagy could potentially be associated with the formation and maintenance of cysts[69]. In addition, increased autophagic activity may have other deleterious consequences: for instance, excessive autophagy in fibroblasts has been shown to release collagen and contribute to tissue fibrosis, a common morphological feature observed in ADPKD[70]. These differences can be explained by a variety of factors, including variations depending on the models used, different autophagic status or varying stages of PKD. Overall, available studies show that dysregulated autophagy plays a significant role in PKD progression in a multifaceted, yet incompletely understood, way as illustrated in **Figure VI**.

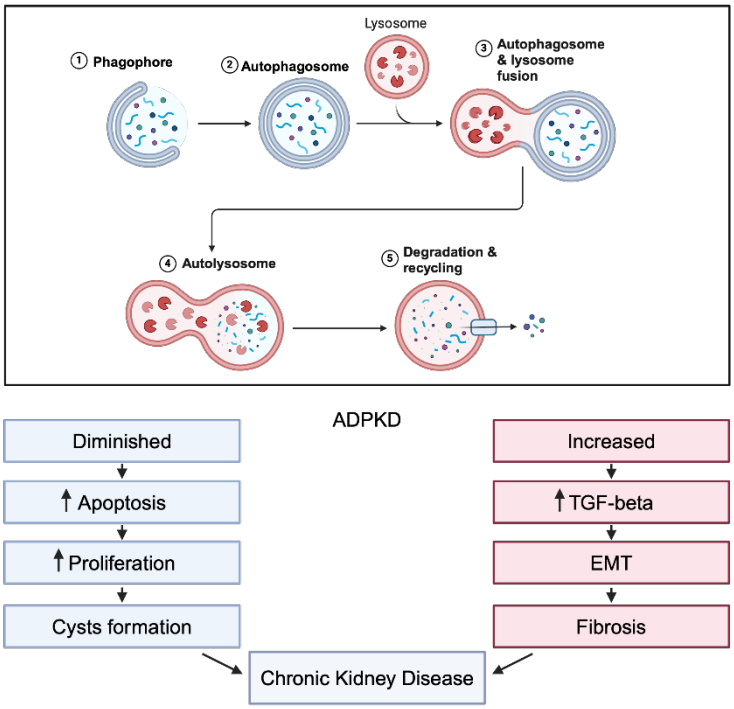

Figure VI. The role of autophagy in ADPKD. In the case of defective autophagy, there is increased apoptotic activity, leading to kidney cell proliferation and cyst formation in ADPKD, eventually leading to chronic kidney disease (CKD). In case of excessive autophagy, there is increased expression of TGF-β1, which induces epithelial-mesenchymal transition (EMT), interstitial fibrosis, and CKD.

Image created with Biorender and adapted from[71].

Aim of the study

This project is part of the Excellence Project of the Department of Medical Sciences of the University of Turin (grant No.#D15D18000410001), which aimed to exploit novel technologies to improve knowledge on disease mechanisms. The aim was to set up functional models that could help refine variants classification. Through a multidisciplinary cooperative effort, involving nephrologists and geneticists working at the local University hospital, we built an analytical pipeline to identify patients with CKD and a clinical suspicion of a monogenic condition. Clinical exome sequencing (CES) followed by an *in-silico* analysis of a panel of CKD-related genes was offered to these patients. After almost 6 years of activity, we have studied >1,200 CES from kidney patients, 279 of whom with a clinical phenotype of “cystic kidneys”. Within the cohort, 60 patients were <18 years old (21.5%) at the time of diagnosis (**Figure VIIA**). Genetic analysis of an *in-silico* panel of cystogenes detected at least one variant in a gene compatible with the clinical phenotype in 232 patients (83.2%), while in the remaining 47 patients (15.1%) genetic analysis was negative or inconsistent, meaning that CES identified no variants or variants in genes unrelated to clinical phenotype, therefore excluded (**Figure VIIB**). 135 patients presented variants in *PKD1* (58.2%), 28 in *PKD2* (12.1%), 8 in *PKHD1* (3.4%) (**Figure VIIC**). Looking at these data, a number of considerations can be drawn: i) *PKD1* is the most recurrently mutated gene, in line with the literature; ii) a significant proportion of the variants identified in *PKD1* (31.9%) were classified as variants of unknown significance (VUS, also called C3) (**Figure VIID**), meaning that their impact in determining the clinical phenotype remains to be defined, iii) the most frequent type of variant is missense (42.2%) (**Figure VIIE**). This is a crucial point since the lack of functional evidence makes the real impact of the variant difficult to evaluate, highlighting the need of rapid and reliable assays for the functional validation of variants of uncertain significance. Finally, when looking at variant distribution along the gene, it appears that there are some exons which are more frequently mutated, including exons 15-18-23-46, representing mutational hotspots. Specifically, CES identified 32 variants in exon 15 (which is also the largest exon) that codes for the majority of PKD extracellular domains and 10 variants in exon 23 that codes for another extracellular domain of PC-1, called REJ domain, where a specific proteolytic site relevant for a correct biogenesis and trafficking of the protein is located.

As mentioned in the introduction section, the impact of *PKD1* variants on the phenotype is incompletely understood. This is particularly true for patients with a negative family history,

who may receive an initial diagnosis by chance, through ultrasound imaging often performed for other reasons, and may obtain a genetic diagnosis, but do not really know what to expect from the disease in terms of progression.

The aim of my thesis has been to generate relatively rapid and easy to use cellular models where specific *PKD1* variants may be reproduced and evaluated. By using CRISPR/Cas9 techniques, we generated homozygous and heterozygous HEK293T cell lines carrying nonsense mutations in exon 15 of *PKD1* ($Ex15^{-/-}$ and $Ex15^{+/-}$). These cell lines represent a pre-requisite for our foremost goal, which is to create a library of cell lines expressing *PKD1* missense variants of unknown significance and to determine their functional impact on the clinical phenotype. This thesis provides a proof of principle of the feasibility of the project, as we managed to introduce a C4 missense variant on exon 42 of *PKD1* gene [c.11614G>A p.(E3872K)] using Cytosine Base Editor in homozygosity both in *PKD1* WT ($Ex15^{+/+}$) and in $Ex15^{+/-}$ heterozygous cells. The latter cell line ($Ex15^{+/-}/Ex42^{M/M}$) should recapitulate what is observed in patients, where cysts usually carry mutations in both *PKD1* alleles, often of different nature (nonsense and missense) and in different location[37]. We then sought to validate the cellular model and most importantly to highlight potential differences that may depend on the nature and on the location of the variant of interest (exon 15 and exon 42 in our case). This thesis reports on the generation and functional characterization of these models.

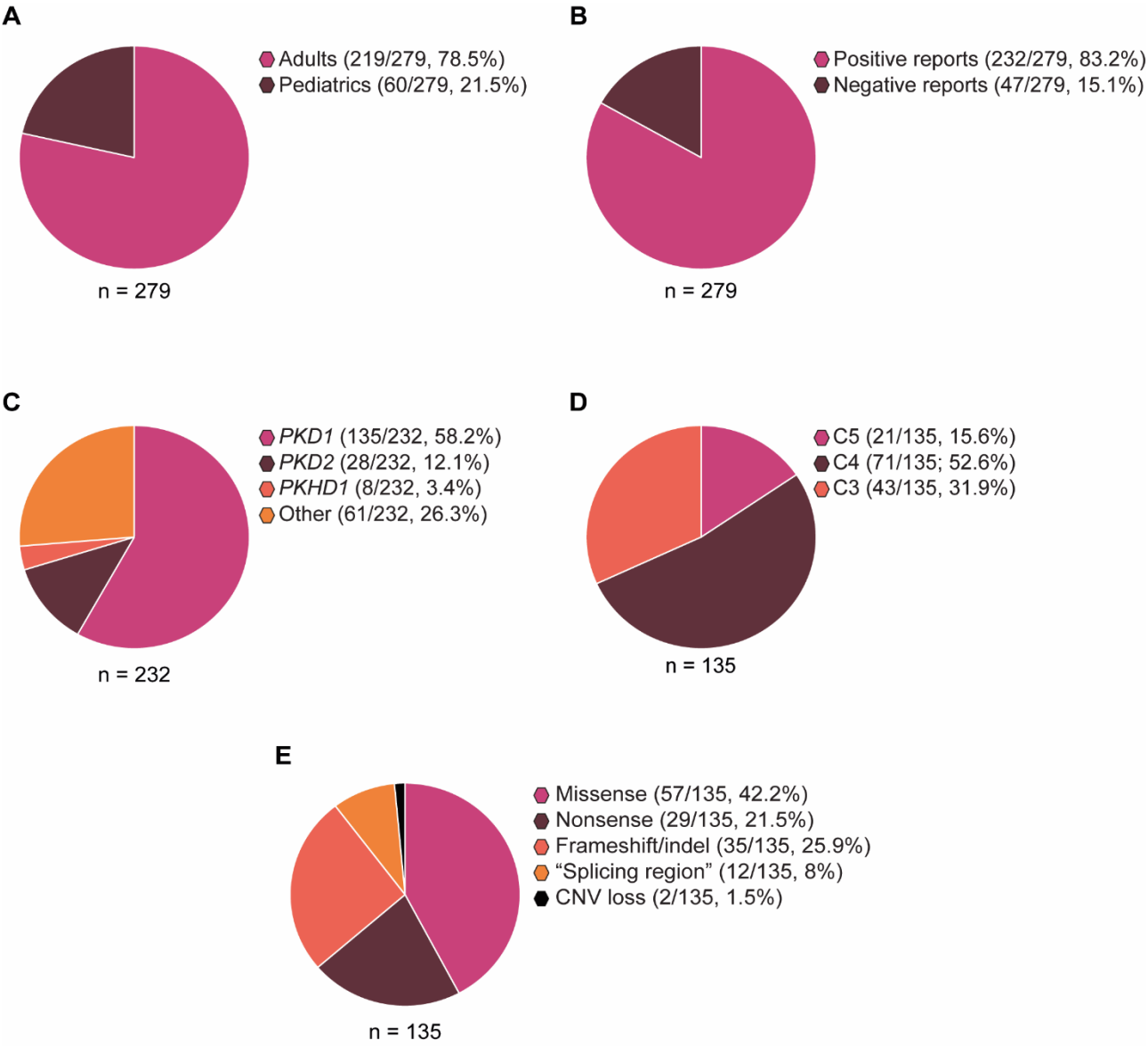

Figure VII. Description of the PKD cohort. (A) Patients' distribution based on their age. (B) Patients' distribution based on the positive or negative outcome of the NGS analysis. Positive reports are those cases where at least one causative variant was identified. (C) Variants' distribution in different PKD related genes. (D) ACMG classification of variants identified in *PKD1* through NGS analysis. (E) Type of variants identified in *PKD1* gene.

Materials and Methods

Cell cultures

Human embryonic kidney (HEK293T) cells were maintained at 37°C in 5% CO_2 in RPMI (#11875093, Thermo Fisher Scientific, Waltham, MA) supplemented with 10% fetal calf serum (FCS). Starving conditions required RPMI supplemented with 0.1% FCS.

Generation of inducible Cas9 cell line

HEK293T cells were infected with a viral vector containing pCW-Cas9 (#50661, Addgene, Watertown, MA) vector and subsequently selected based on antibiotic resistance. Infection efficacy was verified through Western Blot, using monoclonal antibody targeting Cas9 (#MA1-201, Thermo Fisher Scientific).

Generation of *PKD1* knock-out cell line targeting exon 15 and exon 42

A single-guide RNA (sgRNA) was used to target exon 15 of the *PKD1* gene designed by[72], and cloned into the pLX-sgRNA-BfuAI-2k (#112915, Addgene). sgRNA containing vector was transfected into HEK293T, after induction of Cas9 expression using doxycycline (D9891, Sigma-Aldrich, St. Louis, MO), using Lipofectamine 3000 (#L3000001, Thermo Scientific) Introduction of c.11614G>A p.(E3872K) was achieved through Cytosine Base Editor (CBE) (pCMV_AncBE4max_P2A_GFP #112100, Addgene). sgRNA was manually designed and off- and on- target effects were evaluated trough IDT online tool (https://eu.idtdna.com/site/order/designtool/index/CRISPR_SEQUENCE). After co-transfection of sgRNA containing vector (pLKO5.sgRNA.EFS.tRFP , #57823) and the CBE, cells were sorted based on the expression of GFP and RFP through a SH800S cell sorter (SONY) using 130-µm microfluidic sorting chip. sgRNA design and Cas9 plasmid used in this experimental set-up are listed in Table 1. Sanger sequencing of exon 15 and 42 was used to screen the multiple generated clones and to identify the homozygous ones. Concerning the compound heterozygous cells ($Ex15^{+/-}/Ex42^{M/M}$), in line with the goal of the work and for our scientific purposes, we screen the clones to identify those cells carrying the variants *in trans* in the two exons. To this aim, selecting the homozygous clones on exon 42 was the easiest way to achieve this objective.

RNA sequencing

RNA quality was assessed by Bioanalyzer high sensitivity RNA analysis (#5067-1535, #5067-1513 and #5067-1514, Agilent, Santa Clara, CA). Libraries were prepared using the

Illumina Stranded Total RNA Prep with Ribo-Zero Plus (#20040525, Illumina, San Diego, CA) following manufacturer's protocol.

DGE analysis, PCA and UpsetPlot

Differential gene expression (DGE) analysis was performed using the DESeq2 R package (v1.42.0)1. Raw read counts were used as input to generate the log2 fold changes, p-values and adjusted p-values applying default parameters. Shrinkage of effect size was performed using the lfcShrink function (apeglm). Differences in gene expression were considered significant for adjusted p-values < 0.01 and log2 fold change > 1 or < -1. Each clone was compared with a control condition ($Ex15^{+/+}$ either in starving or basal condition). Analyses were corrected to consider a possible batch effect.

Principal component analysis (PCA) was performed through the PCAtools R package (v2.14.0) by plotting the first two components, which accounted for the 24% and the 16.9% of the variance among all clones, respectively. Variance stabilizing transformation (vst) was applied to raw counts (blind = False). Among 27,971 genes, only 14,644 were plotted, as genes with raw counts of at least 10 in at least 6 samples were retained.

UpsetPlots were generated through the ComplexHeatmap package by the UpSet function, to find common DEG among the different comparisons.

Gene ontology (GO) analysis

Gene ontology (GO) analysis was performed by using the enrichR R package (v3.2), by considering differentially expressed genes with an adjusted p-values < 0.01 and log2 fold change > 1 or < -1. For two comparisons ($Ex15^{+/+}$/$Ex42^{M/M}$ vs $Ex15^{+/+}$, both at starving and basal condition) a p-value <0.05 was instead applied. The MSigDB_Hallmark_2020 dataset was used for the analyses. GO terms with a p-value < 0.05 were retained and plotted through the ggplot2 R package (v3.4.4).

Heatmaps

Sub-heatmaps were generated through the ComplexHeatmap R package (v2.18.0) by plotting Z-score-normalized TPMs. Genes with average TPM expression <1 were removed. The average value between two replicates was plotted, and k-means clustering was instead used as clustering method for rows. Sub-heatmaps were generated by plotting the genes belonging to the pathways of apoptosis, adhesion (together with focal adhesion), cell cycle and autophagy (together with mTOR pathway) from PathCards (https://pathcards.genecards.org/).

R version 4.2.2 Patched (2023-02-20 r83916 ucrt).

Genomic DNA extraction and LR-PCR

Genomic DNA was extracted by single clones using DNeasy Blood & Tissue Kit (#69504, Qiagen, Hilden, Germany) and quantified using Nanodrop (Thermo Fisher Scientific).
Exon 15 and Exon 42 of *PKD1* were amplified according to previously described protocol[73] trough Long Range PCR using the Expand Long Range, dNTPack kit (#ELONGN-RO, Roche, Basel, Switzerland) with primers listed in Table 2. After purification of PCR products using QIAquick PCR Purification Kit (#28106, Qiagen), exon 15 was further amplified using a specific pair of primers listed in Table 3. Eurofins (MWG Operon, Ebersberg, Germany) service and analyzed manually.

RNA extraction and RT-PCR

RNA was extracted using RNeasy Plus Mini kit (#74136, Qiagen) and converted to cDNA using the High-Capacity cDNA Reverse Transcription kit (#4368814, Thermo Fisher Scientific). qRT-PCR was performed using the CFX384 Real-Time System (Bio-Rad, Hercules, CA). Primers for *ID2* (Hs04187239_m1), and *GAPDH* (Hs02786624_g1) were from Thermo Fisher Scientific. For *PKD1* transcript, qRT-PCR was performed using iTaq Universal SYBR Green supermix (Biorad). The primers used were 5′-CAAGACACCCACATGGAAAC-3′ (forward in exon 34) and 5′-TGGGGCTGTTCCCAGTTCA-3′ (reverse in exon 35)[52] and for *B2M* 5'-ATGAGTATGCCTGCCGTGTGA-3' (Forward) and 5'-GGCATCTTCAAACCTCCATG-3' (Reverse). Reactions were done in triplicate from the same cDNA (technical replicates). The difference (ΔCT) between the target gene CT (cycle threshold) and *GAPDH* or *B2M* CT was calculated, multiplied by 10^5 obtaining the copy number of the target genes, as described in previous works[74].

Reagents and antibodies

For autophagic flux experiments, Chloroquine (#C6628, Sigma-Aldrich) was added to the cell culture with a final concentration of 100 uM for 5 hours prior to cell lysis.

Primary antibodies used in this work are listed in Table 4.

For Western blot analysis, the following secondary antibodies were used: donkey anti-rabbit IgG-horseradish peroxidase (HRP) - conjugated (#NA934V, GE Healthcare, Milan, Italy), goat anti-mouse IgG HRP-conjugated (#NA931V, Perkin Elmer, Milan, Italy).

For Immunofluorescence analysis, Alexa Fluor 488 goat anti-rabbit IgG (#A11008) was used as secondary antibody. Fort actin cytoskeleton and nuclei staining, Alexa Fluor 647 Phalloidin (#A22287) and 4′,6-diamidino-2-phenylindole (DAPI, #D3571) (all reagents from Thermo Fisher Scientific) were used, respectively.

Apoptosis and cell cycle analysis

Cells, either cultured in complete or starving medium for 68 hours, were collected and viability assessed by Annexin V-APC Apoptosis Kit (#2620475, Thermo Fisher Scientific) following manufacturer's instructions. For cell cycle analyses, cells were cultured either in complete or starving medium for 24h and 48h. Collected cells were then fixed with cold ethanol (70%) for 1h. PI-based staining was performed using FxCycle PI/RNase Staining Solution (#F10797, Thermo Fisher Scientific). Samples were analyzed by flow cytometry using FACS Celesta (BD Bioscience, Milan, Italy).

Western Blot

Cells were lysed (150 mM NaCl, 20 mM HEPES [pH 7.4], 50 mM NaF, 1 mM Na_3VO_4, 1 mM EGTA, 50 µM phenylarsine oxide, 10 mM iodoacetamide, 1 mM PMSF, and 1% NP-40) and nuclear debris was discarded by centrifugation (20'000*g*, 15 minutes). For cytoplasmic-nuclear separation, cells were grown either in basal or in starving medium for 48h before collection. Nuclear–cytoplasmic fractionation was conducted using the NE-PER Nuclear and Cytoplasmic Extraction Reagents kit (#78833, Thermo Fisher Scientific) according to the manufacturer's protocol. Proteins were resolved by SDS-PAGE gels and transferred to nitrocellulose membranes (Bio-Rad).

For Polycystin-1 visualization, cells were lysed in RIPA buffer (150 mM NaCl, 0.5% DOC, 0.1% SDS. 50 mM Tris [pH 7.9] and 1% Triton X-100) and then proteins were resolved by 3-8% Tris-acetate gels (#EA0375PK2, Thermo Fisher Scientific) and transferred to PVDF membranes (#88518, Thermo Fisher Scientific).

After incubation with primary and secondary antibodies, images were acquired using the ChemiDoc Touch Imaging System. Densitometric analyses were performed with Image Lab Software (both from Bio-Rad).

Immunofluorescence staining

Cells cultured on coverslips (either treated or not treated with Poly-L-lysine #P4832 or fibronectin 10ug/ml #F0895 from Sigma-Aldrich) were rinsed briefly with PBS and then fixed with PFA 4% for 10 minutes. Fixed cells were then permeabilized with 0.1% Triton X-100 in

PBS or with saponin 0.1%. Nonspecific binding was blocked with 1% or 5% BSA in PBS for 30 minutes, after which primary antibodies were applied and incubated for 1 hour at room temperature or overnight at 4°C. Subsequently, slides were washed with PBS, incubated with secondary antibodies conjugated to fluorophores for 45 minutes, and washed again with PBS. Finally, nuclei were stained with DAPI and then coverslips were observed under an inverted confocal microscope (Leica sp5 or sp8).

Autophagic flux analysis

Cells were transduced using a Premo autophagy tandem sensor mCherry-GFP-LC3B kit (#P36239, Thermo Fisher Scientific) to monitor autophagic flux. Autophagy was then induced by serum deprivation for 24h. Choloroquine (90 uM) was added to the medium for 16 hours as a control of autophagosome formation. Cells were then fixed, permeabilized and stained with DAPI. Confocal images were taken using Leica sp5. Analysis was performed using ImageJ's tool JaCOP considering threshold adjusted Manders coefficients as colocalization parameter.

Statistical analyses

Results were analyzed using un-paired parametric t test. Statistical analysis was performed using GraphPad Prism 8.0.2 (GraphPad Software, La Jolla, CA).

Results

Establishment of the cellular model to reproduce *PKD1* variants

To investigate the genotype-phenotype correlation of *PKD1* variants identified in our cohort, we developed a cellular model using HEK293T cell line genetically modified through CRISPR/Cas9 technology. We transfected HEK293T cells with the pCW-Cas9 lentiviral vector encoding an inducible Cas9-cell and a puromycin-resistance element. Western blot analysis of selected cells was used to validate target expression (data not shown). After Cas9 induction, cells were transfected with a sgRNA-expressing plasmid (pLX-sgRNA-BfuAI-2k), targeting exon 15 of *PKD1*[72] to generate both heterozygous and homozygous mutants, $Ex15^{+/-}$ and $Ex15^{-/-}$, which all carry truncating variants. Cells were also transfected with empty vectors to generate WT clones, used as negative control ($Ex15^{+/+}$). According to literature reports, the progression of ADPKD is in line with a "double hit" model, which means that inactivation of both *PKD1* alleles by germline and somatic variants is necessary for the cystic phenotype to manifest. For this reason, $Ex15^{+/+}$ (*PKD1* WT) and $Ex15^{+/-}$ clones were then used to introduce a specific additional variant, c.11614G>A p.(E3872K) in exon 42, using cytosine base editor (CBE). Cells were then sorted and plated at single-cell level. Sanger sequencing of exon 42 was the selected technique to screen the multiple generated clones and to identify only homozygous ones (schematic representation of the generation of the clones is depicted in **Figure 1A**). All stop-codon variants introduced in exon 15 target an important extracellular domain of PC-1 (PKD repeats), while the missense variant induced an aminoacidic change (p.E3872K) in one of the transmembrane (TM) regions towards the end of the protein (**Figure 1B**). The substitution of the glutamate into a lysine should disrupt a hydrogen bond that links the oxygen of the carboxylic group of the glutamate to the amine group of the backbone (dashed yellow line), resulting in a structural destabilization of PC-1 (**Figure 1C**).

After Sanger sequencing confirmed the presence of the variants (**Figure 2A**), we evaluated firstly *PKD1* transcript levels - which did not show any statistical differences between clones and WT cells (**Figure 2B**) – and PC-1 level through Western Blot. A full-length form of PC-1 (FL) was detected by western blot in $Ex15^{+/+}$ cells (**Figure 2C**), halved in heterozygous clones ($Ex15^{+/-}$), while no FL-PC-1 was observed in full knock-out clones ($Ex15^{-/-}$). Of note, truncating mutations in exon 15 led to the formation of a putative truncated form of the protein (arrow), probably because the introduction of a truncating variant on exon 15 does not necessarily imply RNA-mediated decay of *PKD1* transcript, which was still produced and

coded (potentially) for a shorter and non-functional protein. On the contrary, the introduction of the missense variant c.11614G>A did not apparently affect the protein level in either $Ex15^{+/+}/Ex42^{M/M}$ and $Ex15^{+/-}/Ex42^{M/M}$, as we were able to detect FL-PC-1 in these clones too.

DEG and GO analyses reveal dysregulation of terms related to ADPKD both in $Ex15^{-/-}$ and $Ex15^{+/-}/Ex42^{M/M}$

Once we confirmed that the expression of PC-1 was consistent with the genetics of the generated cell lines, we performed a RNA sequencing to identify the pathways that are differentially expressed in $Ex15^{-/-}$ and $Ex15^{+/-}/Ex42^{M/M}$ clones compared to the WT cells. Clones were cultured both in a complete medium (basal) and in starving condition (48h; 0.1% FCS) to mimic the induction of ciliogenesis, as demonstrated by Tang and colleagues, who showed that serum starvation-induced autophagy promotes this process through selective degradation of the satellite pool of the OFD1 protein, encoded by the gene responsible for OFD type I syndrome[75].

An initial Principal Component Analysis (PCA) demonstrated that the two biological replicates used for the subsequent analyses are equivalent and it also highlighted a clear distinction between the two different culturing conditions – basal and starving – as underlined by the dashed line in **Figure 3A**. Moreover, both in basal and in starving conditions, a different clusterization among the clones was highlighted, reflecting their genetics. Specifically, $Ex15^{+/+}$ and $Ex15^{+/+}/Ex42^{M/M}$ clones grouped together, suggesting a similar overall expression pattern. Likewise, $Ex15^{+/-}$, $Ex15^{-/-}$ and $Ex15^{+/-}/Ex42^{M/M}$ clones clustered together, but distant from the other twos. A similar pattern of distribution is observed either in basal or serum-deprived conditions.

We next focused on the differentially expressed genes (DEG) of each clone compared to the WT cells (**Figure 4A, B**). In basal conditions, $Ex15^{-/-}$ clones presented 73 up-regulated and 66 down-regulated genes compared to WT cells (**Figure 4A**). Among them, 54 up-regulated and 35 down-regulated were not shared with other clones, representing a unique feature. GO analysis performed on this subset of genes highlighted EMT, p53 pathway, KRAS signaling and IL-2/STAT5 pathway within the up-regulated group of genes. On the contrary, when looking at the down-regulated ones, terms related to regulation of intrinsic apoptotic signaling pathway, as well as of endothelial cell-matrix adhesion via Fibronectin and eventually negative regulation of autophagy were observed.

A similar analytical approach was exploited to more deeply characterize the $Ex15^{+/-}/Ex42^{M/M}$ clone. A unique signature of 204 up-regulated and 248 down-regulated genes was identified compared to the WT clone. G_2-M checkpoint, EMT, Glycolysis and Fatty acid metabolism were mainly present within the upregulated subset, while p53 pathway, Myc Targets and Unfolded Protein Response were mainly enriched in the down regulated group.

In starving conditions, 223 up- and 139 down-DEGs were uniquely present in $Ex15^{-/-}$ compared to WT (**Figure 4B**). EMT, Apical Junction, TGF-beta signaling, cell adhesion molecules and Focal adhesion were the main process enriched in up-regulated subset, while terms related to apoptosis, cell-cell junction, adherens junction and zonula Adherens characterized the down-regulated ones. On the contrary, genes that were differentially expressed and only found in $Ex15^{+/-}/Ex42^{M/M}$ cells compared to the control were associated to terms such as EMT, Glycolysis for the up-regulated ones, whilst Myc Targets V1, IL-2/STAT5 Signaling, TNF-alpha Signaling via NF-kB were down-regulated. In summary, the initial DEG analyses highlighted GO terms related to ADPKD, such as EMT, p53 pathway, cell-matrix adhesion and autophagy, which seemed to be dysregulated in $Ex15^{-/-}$ and $Ex15^{+/-}/Ex42^{-/-}$ compared to $Ex15^{+/+}$. Some terms were shared (such as EMT, p53, Myc targets), but others were not (i.e. Glycolysis and Fatty acid metabolism), suggesting that the introduction of the missense variant may be causative of these discrepancies.

Finally, GO analysis was performed on all up- and down-regulated genes that are shared among the clones to understand whether these genes may contribute to the pathological phenotype (**Figure 4C, D**). Overall, the transcriptional landscape did not undergo radical changes, implying that the DEGs uniquely found in each clone are the main contributors to the phenotype. Nonetheless, an enrichment of the mTORC1 and ROS pathway was found in $Ex15^{-/-}$ vs $Ex15^{+/+}$ (**Figure 4C**). In starving conditions, the additional shared DEGs equally contributed to the same signatures previously mentioned for $Ex15^{-/-}$ vs $Ex15^{+/+}$ and $Ex15^{+/-}/Ex42^{M/M}$ vs $Ex15^{+/+}$ (**Figure 4D**). All genes found associated with each GO term are listed in Table 5 and 6.

To sum up, DEG and GO analyses highlighted those terms that may be related to the pathogenetic mechanisms of ADPKD, providing evidence of the validity of the models and the basis for functional validation experiments.

Differential expressed genes underline pathway-specific differences among clones

DEG and GO analyses depicted an overall picture of the generated clones that reflects typical features of the pathology, including those pathways that are the most disrupted in

ADPKD as extensively addressed in the introduction section. For this reason, we sought to investigate deeply the main altered cystogenic pathways to unravel the key genes responsible for a certain phenotype. The selected pathways (Cytoskeleton, Cell-adhesion, Cell Cycle and Autophagy) were investigated considering the genes that were differentially expressed in $Ex15^{-/-}$ and $Ex15^{+/-}/Ex42^{M/M}$ vs $Ex15^{+/+}$.

Regarding cytoskeleton, the most interesting differences and similarities among clones are observed in basal condition. As a matter of fact, genes involved in actin depolymerization, such as *LIMK1* and *CFL1*[76], were found to be more expressed in $Ex15^{-/-}$, $Ex15^{+/+}/Ex42^{M/M}$ and $Ex15^{+/-}/Ex42^{M/M}$. Moreover, *TIAM1* is overexpressed compared to WT cells which is thought to alter actin organization and cellular shape and is associated with changes in Rac1/RhoA/ROCK signaling activity, also suggested by the lower expression of *ROCK1* in the same clones (**Figure 5A**)[77]. Lastly, it is noteworthy that genes involved in F-actin outgrowth and focal adhesion formation[78] (*ENAH* and *ARPC5*) were down-modulated in $Ex15^{-/-}$.

It has long been recognized that alteration of ECM components and cell-adhesion properties is a striking event during cysts development. Extensive evidence demonstrated that cysts in human ADPKD kidneys had thickened and laminated cellular basement membranes as well as an abnormal regulation of gene expression of several ECM components, including collagens, laminins and proteoglycans by cyst epithelial cells[79]. Indeed, expression of *ITGB8*, *ITGB4*, *COL4A1*, *COL4A2*, *COL6A2*, *ITGA1*, *LAMA5*, *SDC1* and *ITGA8* is higher in $Ex15^{-/-}$ and $Ex15^{+/-}/Ex42^{M/M}$ clones compared to WT cells (**Figure 5B**).

Among the different types of cell-matrix interactions, focal adhesions play an important role in cyst progression. As a matter of fact, Joly et al.[45] showed that overexpression of a PC-1 C-terminal fragment in collecting duct cells stimulated the phosphorylation of FAK and paxillin, leading to the formation of focal adhesion complexes. Thus, it is possible to speculate that the loss of PC-1 during renal development causes to abnormal turnover of focal adhesions. Several genes involved in the assembly of FAs are deregulated also in our clones: for instance, *CRK* was found down-regulated in both $Ex15^{-/-}$ and $Ex15^{+/-}/Ex42^{M/M}$ clones, while *PTK2* and *CAPN2* are negatively modulated only in $Ex15^{-/-}$ (**Figure 5B**).

Looking at the specific heatmap of genes involved in cell cycle regulation (**Figure 5C**), we may observe a trend of similar expression between $Ex15^{-/-}$ and $Ex15^{+/-}/Ex42^{M/M}$ clones in basal conditions. Specifically, genes as *POLA2*, *CCND1* and *CCNB2*, whose function converge in promoting proliferation and DNA replication, are more expressed compared to

the other three clones. Anyhow, when switching to the starving conditions, their expression is kept higher only in full Ex15$^{-/-}$ clones.

As regarding the autophagic pathways, there are some dysregulated genes that suggest a potential defect in this peculiar process in Ex15$^{-/-}$ and Ex15$^{+/-}$/Ex42$^{M/M}$ clones (**Figure 5D**). For example, in basal conditions we see a lower expression of three mTOR inhibitors, such as *PRKAA2, DDIT4* and indirectly *RHEB,* suggesting a hyperactivation of mTOR activity. Moreover, several genes involved in endosomal trafficking and autophagosomal maturation are poorly expressed, as *RAB39A*, *RAB35*, *RAB9A* and *RAB4A*.

All together, these results showed that, concerning the main pathways disrupted in ADPKD, our clones presented a differential expression pattern, with an overall overlapping between Ex15$^{-/-}$ and Ex15$^{+/-}$/Ex42$^{M/M}$ clones, but still a functional assessment of these processes is needed to fully confirm the validity of the models.

Ex15$^{-/-}$ and Ex15$^{+/-}$/Ex42$^{M/M}$ clones show defective actin polymerization and disrupted formation of focal adhesions

Based on RNA-sequencing results, selective functional assays were performed to test the impact of the different *PKD1* variants generated on the pathological phenotype.

When considering cytoskeleton organization, we evaluated the capacity of the different clones to polymerize actin filaments in basal conditions. We plated cells on untreated coverslips overnight and then stained with phalloidin and DAPI to visualize actin and nuclei. As expected, WT cells showed a normal actin polymerization ability which can be assumed by the number of actin filaments produced in basal condition. No significant differences were observed in Ex15$^{+/-}$ and in Ex15$^{+/+}$/Ex42$^{M/M}$ cells, implying that the missense variant on exon 42 alone is not able to impair this process. In contrast, cells lacking FL-PC-1 (Ex15$^{-/-}$) showed a defective actin polymerization instead, as the filaments count is lower compared to the WT cells. Interestingly, the behavior of cells expressing a heterozygous variant in exon 15 and a homozygous variant on exon 42 (Ex15$^{+/-}$/Ex42$^{M/M}$) overlapped with that of Ex15$^{-/-}$ cells, indicating that the sum of the two variants disrupts actin polymerization abilities. This data led to the hypothesis that the region of the protein where the mutation falls is somehow involved in the regulation of actin cytoskeleton and adhesion properties of the cells (**Figure 6A**).

To further dissect this phenomenon, we evaluated the possibility of a defective formation of focal adhesions (FAs) underlying an altered cell adhesion and a reduced capacity to

polymerize actin. For this purpose, we starved the cells overnight and we plated them on coverslip previously treated with fibronectin. Fibronectin interacts and activates cell surface integrins that in turn recruit a series of cellular proteins involved in connecting with the actin cytoskeleton inside the cell: this initiates the formation of the integrin-based adhesive organelles that are FAs. Intracellular signaling elicited by integrins or growth factor receptors initiates the phosphorylation of FAK (also called *PTK2*) at tyrosine 397 (Y397) that is a critical for c-Src binding and FAK itself activation[80]. The activated FAK/c-Src complex can phosphorylate the downstream signaling molecules and the cytoskeleton-associated proteins, promoting and regulating multiple cellular processes, as cell adhesion, migration, proliferation and survival[81]. We therefore stained with an antibody against phospho-FAK to highlight active FAs (**Figure 6B**). In line with the actin polymerization process, $Ex15^{+/+}$, $Ex15^{+/-}$ and $Ex15^{+/+}/Ex42^{M/M}$ cells were able to properly form FAs, with accumulation of phopsho-FAK signal (green) at the top of actin filaments. On the contrary, $Ex15^{-/-}$ and $Ex15^{+/-}/Ex42^{M/M}$ were significantly less positive for p-FAK1, with most of the molecule being retained in the cytoplasm rather than localized at the adherent points.

Taken together, these results indicate that the variant on exon 42 of *PKD1* alters actin remodeling and FAs formation only when coupled with a more deleterious mutation that hits the extracellular portion, giving a similar phenotype to what we observed in a full knock-out clones on exon 15.

In a serum-deprived condition, $Ex15^{-/-}$ clone enters in S/G_2 phases more easily than other clones due to the induction of Id2

Previous works demonstrated that cystic cells are characterized by a higher proliferation rate as loss of *PKD1* or *PKD2* promoted cell-cycle progression to S and G_2 phases. Several authors[82,83] linked the abnormal epithelial proliferation observed in cystic kidneys to the upregulation of the transcriptional regulator inhibitor of differentiation 2 (Id2), which triggers an Id2-mediated downregulation of p21 in both kidneys of *PKD1/2* patients and in *pkd1* knockout mice (schematic representation of how PC complex interacts with Id2 regulating S/G_2 entry is depicted in **Figure 7A**). Based on this knowledge and based on RNA-seq data showing that terms related to cell cycle and proliferation pathways were de-regulated in the generated clones compared to $Ex15^{+/+}$, we investigated whether our mutant cells lines behave similarly to what happen in patients' cells and murine PKD models. Cells were cultured both in complete and in serum-deprived medium for 48 hours before cell cycle analysis. Results indicate that in complete medium there are no significant differences

between clones (neither in terms of G_0/G_1 nor S/G_2), however, in a serum-deprived medium $Ex15^{-/-}$ cells showed a significant increase in percentage of cells in the S/G_2 phases compared to WT clones. All other clones - $Ex15^{+/+}/Ex42^{M/M}$ and $Ex15^{+/-}/Ex42^{M/M}$ - showed a slight but not significant increment in S/G_2 cells compared to the WT (**Figure 7B**), meaning that the aberrant proliferation could be a prerogative of $Ex15^{-/-}$ clones only.

We then evaluated the transcription, translation and cellular localization of *ID2* and its protein product (Id2), a member of helix-loop-helix family of transcription factors, which notably acts as a positive regulator of cell proliferation. RT-PCR data indicated that *ID2* levels significantly decreased when switching from basal to starving conditions in $Ex15^{+/+}$, $Ex15^{+/-}$ and $Ex15^{+/+}/Ex42^{M/M}$, indicating that cells arrested themselves in G_0/G_1 phases. On the contrary, in $Ex15^{-/-}$ cells, *ID2* transcript levels remained significantly higher than those of $Ex15^{+/+}$ cells, potentially explaining why $Ex15^{-/-}$ cells kept on progressing towards S/G_2 phases (**Figure 7C**). We next evaluated the expression of Id2 protein in whole cell lysates showing that $Ex15^{-/-}$ and $Ex15^{+/-}/Ex42^{M/M}$ in basal conditions produce larger amounts of Id2 compared to WT cells, even though no difference in terms of cell-cycle alteration was appreciated in this experimental set-up. After 48 hours of starving, Id2 levels drastically dropped in all clones compared to the basal condition (red asterisks). However, $Ex15^{-/-}$ cells maintained a higher Id2 expression compared to $Ex15^{+/+}$ cells, explaining the greater portion of cells in S/G_2 phases in these conditions. To further corroborate these findings, we performed western blot analyses on cytoplasm-nuclear lysates in the same culturing condition to see whether there was a different distribution of Id2 between these two cellular compartments. In fact, the Id2-mediated increment of S-phase entry in *PKD1* mutant cells should require the translocation of the protein from cytoplasm to the nucleus, as it exploits its function in potentially three different ways: (1) through binding with Rb to control Rb-E2F-mediated S-phase entry; (2) through binding with bHLH factors to inhibit transcription of *CDKN1A* gene; (3) through inhibition of p21 to increase Cdk2/Cdk4-mediated phosphorylation of Rb (**Figure 7A**)[83]. In basal conditions, in $Ex15^{+/+}$ and $Ex15^{+/-}$ cells most of the protein was in the cytosol, suggesting an inactive state. In $Ex15^{-/-}$ clones, Id2 level is higher compared to $Ex15^{+/+}$ both at cytosolic and nuclear level with no significant difference between the two cellular compartments. As concerning $Ex15^{+/+}/Ex42^{M/M}$ cells, they showed a significant increase in Id2 protein level too, but only in the nuclear section compared to $Ex15^{+/+}$.

In starving conditions, we observed that Id2 level in $Ex15^{+/+}$, $Ex15^{+/-}$, $Ex15^{+/+}/Ex42^{M/M}$ and $Ex15^{+/-}/Ex42^{M/M}$ is maintained low in both cytosol and nucleus in contrast to $Ex15^{-/-}$ where

we demonstrated that not only Id2 levels were significantly increased compared to WT, but also that it translocated more into the nucleus where it could exploit its function, supporting the results obtained from the cell-cycle analyses (**Figure 7D**).

Considered together these results show that cells expressing truncating variants in exon 15 are more resistant to starving conditions, showing a greater percentage of cells in the S/G_2 phases. This behavior may be linked to a greater expression and cytoplasm-nuclear translocation of Id2, which is not appreciated in $Ex15^{+/-}/Ex42^{M/M}$ mutants, meaning that probably the protein domain coded by exon 42 is not involved in regulating Id2 activity.

All homozygous clones ($Ex15^{-/-}$, $Ex15^{+/+}/Ex42^{M/M}$ and $Ex15^{+/-}/Ex42^{M/M}$) show an increased resistance to apoptosis in a stressful environment

Another key pathway that is altered in ADPKD is the apoptotic one. It is widely known that apoptosis is persistently causing the alteration of the renal parenchyma. A number of *in vivo* models showed that the inactivation of *bcl-2* – an important inhibitor of apoptosis – initiates the disease[50,84]. However, $CD133^+$ progenitor cells isolated from human ADPKD patients, when cultured in a serum deprived medium, are characterized by a strong resistance to apoptosis[52]. RNA-sequencing data showed that term related to apoptosis is differentially regulated in all mutant clones and based on this, we wanted to understand how our cells behaved in terms of apoptotic response, both in basal and in starving culturing conditions. As represented by FACS profiles (**Figure 8A**) and by the cumulative graphs (**Figure 8B**), full knock-out ($Ex15^{-/-}$, $Ex15^{+/+}/Ex42^{M/M}$) and compound heterozygous ($Ex15^{+/-}/Ex42^{M/M}$) clones showed a significant increased resistance to apoptosis, which can be observed only in starving condition.

$Ex15^{-/-}$ and compound heterozygous clones fail to convert LC3BI to LC3BII suggesting a potential defective autophagic flux

Extensive studies have dissected the autophagic mechanism in PKD, demonstrating both increased and decreased autophagy activity depending on the different type of experimental models[85,69,86]. Moreover, terms related to mTORC1 pathway emerged during RNA sequencing analyses as down-regulated both in $Ex15^{-/-}$ and $Ex15^{+/-}/Ex42^{-/-}$ in basal condition, suggesting a potential alteration of the autophagic process in these cell lines. To test whether a potential defect in autophagy can be a characteristic trait of our model too, we starved the cells for 48h and assessed the conversion of LC3B isoform I to isoform II, a key step for the formation of autophagosomal membranes. Basal autophagy seemed not to be altered, as expression level of LC3BII is similar across all the clones. When subjected to

starving, LC3BII levels increased significantly in $Ex15^{+/+}$, $Ex15^{+/-}$ and $Ex15^{+/+}/Ex42^{M/M}$, while the full knock-out on exon 15 and the compound heterozygous did not follow the same behavior (with a low conversion of LC3BI to II) (**Figure 9A**). Since LC3BII increment simply indicates the accumulation of autophagosomes and does not guarantee autophagic degradation, western blot on basal and starving conditions is insufficient to determine whether the autophagic flux is defective. If, however, the amount of LC3BII further accumulates in the presence of a lysosomal activity inhibitor, this would indicate the enhancement of the autophagic flux. Given that, we cultured the cells in presence of chloroquine (CQ), an inhibitor of lysosome fusion with autophagosomes. We observed that CQ treatment induced the accumulation of LC3BII in all clones, but to a lesser extent in $Ex15^{-/-}$ and $Ex15^{+/+}/Ex42^{M/M}$, suggesting a potentially defective autophagic flux.

Previous works demonstrated that ADPKD is a condition where an accumulation of autophagic vesicles is observed, suggesting a problem in the fusion of these vesicles with the lysosome[87]. To investigate the late steps of autophagy which consist in the fusion between autophagosomes and lysosomes we used an artificial system based on the infection of our cells with a tandem fluorescent protein construct containing LC3B cDNA that allows an enhanced dissection of the maturation of the autophagosome to the autolysosome[88,89]. By combining an acid-sensitive GFP (Emerald GFP) with an acid-insensitive RFP (TagRFP), the change from an autophagosome (neutral pH) to the autolysosome (with an acidic pH) can be visualized by imaging the specific loss of the GFP fluorescence upon acidification of the autophagosome following lysosomal fusion. Upon induction of autophagy, the Premo Autophagy Tandem Sensor labels the punctate autophagosomes; these structures are positive for both GFP and RFP (yellow). Once the lysosome has fused, the pH drops, which quenches the GFP, making autolysosomes appear red (schematic representation of the experimental workflow is depicted in **Figure 9B**). Cells were plated on coverslips with complete medium and infected with the viral construct for 16 hours before switching to a low-content serum medium for 24 hours. Cells were then fixed, and nuclei stained with DAPI. Co-localization analysis highlighted that in $Ex15^{+/+}$, $Ex15^{+/-}$ and $Ex15^{+/+}/Ex42^{M/M}$ clones the formation of autolysosomes occurs correctly as the fraction of red signal co-localizing with the green one is lower (M2 coefficient, RFP vs GFP). Meanwhile, in $Ex15^{-/-}$ and $Ex15^{+/-}/Ex42^{M/M}$ clones the induction of LC3B expression causes the formation of autophagosomes as indicated by the predominance of yellow puncta over

red ones (higher M2 coefficient). All together, these results confirmed the presence of a defective autophagic flux in $Ex15^{-/-}$ and $Ex15^{+/-}/Ex42^{M/M}$ clones, in line with the disease.

Discussion

Autosomal dominant polycystic kidney disease, the most common genetic cause of kidney failure, is predominantly caused by pathogenic variants in *PKD1* or *PKD2*. Advances in sequencing technology have resulted in an increase in the utility of genetic testing in patients with suspected ADPKD[90]. Clinically, ADPKD is characterized by heterogeneity in presentation and evolution of the disease, with widely different kinetics of progression toward end stage renal failure. There are some indications of a genotype-phenotype correlation, with truncating variants generally associated with a more rapid cyst formation and worsening of kidney function compared to missense mutations[91]. However, it is very difficult to make predictions of disease evolution, particularly if the family history is silent and in the presence of missense variants or in the presence of variants of unknown significance that may be particularly critical to interpret. In addition, recent data indicate that some patients bear more than one *PKD1* mutation or additional rare genetic variants in cystogenes: these variants may act as contributing factors, similar to what has been described for Alport syndrome patients where multiple variants in collagen genes may have additive, neutral or compensating effects[92].

In this context, the foremost aim of our work was to provide a proof of principle that it is possible to generate cellular models carrying *PKD1* variants exploiting novel genome editing approaches useful to provide functional explanation particularly for variants of unknown significance. We initially generated truncating variants on exon 15 (which in our cohort represents a mutational hotspot) exploiting conventional CRISPR/Cas9 technique. Secondly, we introduced a specific missense variant (c.11614G>A;p.E3872K) we identified in one of our patients already reported in Varsome as likely-pathogenic (C4) on exon 42, which induces an aminoacidic change from glutamate to lysine. We chose the aforementioned variant because i) it is a missense variant, which represents the most frequent type of mutation both in our cohort and in larger available databases (on Clinvar, missense variants on *PKD1* are 1222 over 2451 total C3/C4/C5 mutations, 49.9%); ii) it is located in a region with low homology grade with pseudogenes[16], making the editing easier; iii) eventually, it is a single-base substitution that can be modeled with base editors. Base editing is a recent iteration of CRISPR-Cas nuclease editing that can overcome some of the precision limitations of standard nuclease modifications. Base editing results in C>T (and G>A on the complementary strand) changes at the target site in the case of cytosine base editing (CBE) or A>G (and T>C) in the case of adenine base editing (ABE). Like nuclease

editing, BEs consist in a Cas9 bound to a sgRNA containing an RNA scaffold and a 20-nucleotide sequence upstream PAM sequence. The main two differences compared to standard CRISPR system are the fact that (i) the Cas9 is catalytically inactive so that it can only make a single-strand nick and that (ii) it is fused to a cytosine or adenosine deaminase domain. The advantage is that base editing can occur with high efficiency, even in non-dividing cells and does not require an exogenous DNA template to make precise modifications. Besides, even though not all single base substitutions are possible with this technique (indeed, only four out of twelve possible conversions are feasible), it is important to highlight the fact that among the C3/C4/C5 missense variants reported on Clinvar and identified on *PKD1*, 749/1222 (61.3%) variants are caused by substitutions that can be edited by CBE or ABE (data available online https://www.ncbi.nlm.nih.gov/clinvar). However, sgRNA design for this kind of Cas9 is not always practical as different technical requirements need to be fulfilled: the target base must fall in a specific activity window inside the sgRNA (usually between the 4^{th} and the 8^{th} nucleotide); no by-stander bases should be located around the target base and if so, it is necessary to evaluate the impact of its potential substitution on the protein production and function before synthetizing it. However, despite the design difficulties, there are many types of BEs that differ based on the efficiency, the PAM sequence and activity window so that a wide spectrum of editing possibilities is available[93].

Our results suggested the validity of the newly generated cellular model, as RNA sequencing data (and later confirmed by the functional ones) showed transcriptional signatures that are shared with ADPKD phenotype (such as terms related EMT, mTORC, TGF-beta signaling, G_2-M transition etc). It is also true that some of the alterations observed seemed to move in the opposite direction from what previously reported, as in the case of mTORC, p53 and cytoskeleton alterations. This is a major controversial point of the RNA-sequencing results; nonetheless, by dissecting the components of each GO terms, we highlighted a consistency with our functional results, as we deeply discussed in the results section. We believed that there could be driving genes that lead the pathway more than others and specifically with either inhibitory or activating functions, meaning that even if globally the gene expression analysis seemed to be contradictory in our clones, functional assessment was still required.

Concerning the functional part of this work, the assays performed were chosen based both on RNA sequencing data and on the previously published literature. Given the results we obtained, we were able to confirm the pathogenicity of the missense variant c.11614G>A,

as Ex15$^{+/-}$/Ex42$^{M/M}$ clones are both transcriptionally and functionally similar to Ex15$^{-/-}$ - which behave as a positive control – confirming either the validity of the model and the accuracy of the selected assays. This is a key point of the work because it paves the way to a rapid functional evaluation of those variants classified as C3, which make ADPKD diagnosis more difficult and uncertain. Moreover, we can also claim the fact that the "double-hit" hypothesis is true also in our cellular model: indeed, Ex15$^{+/-}$ clones – although transcriptionally similar to the Ex15$^{-/-}$ and Ex15$^{+/-}$/Ex42$^{M/M}$ - functionally resemble WT cells, as the introduction of a truncating heterozygous variant on *PKD1* does not lead to the pathological phenotype (as expected). Nonetheless, it was odd not to observe a pathogenetic profile also in Ex15$^{+/+}$/Ex42$^{M/M}$ clones, as they carry a likely pathogenic variant in homozygosity. The possible explanation to the absence of a clear (or milder compared to Ex15$^{-/-}$) phenotype can be addressed to the fact that this variant was identified in cis with a second additional germline variant in *PKD1* (c.5600A>G p.(N1867S)), precisely on exon 15, meaning that the presence of the first variant alone is probably not sufficient for the clinical phenotype to manifest. This could explain why when combined with a more deleterious variant (such as the truncating one on exon 15) also the missense variant on exon 42 have an impact on the phenotype, in line with the "double hit" hypothesis that explains the disease's progression.

Lastly, a further key point of this work was the possibility to estimate to what extent the type of variant influences the phenotype and if its location along the gene may have a different contributor effect to the pathways' alteration. As one might expect from its large, multi-domain structure and multiple cellular locations, the functions ascribed to PC-1 are numerous but are not completely understood in an integrated or disease-relevant perspective. The truncating variants on exon 15 target an important region of the extracellular portion of PC-1, the PKD repeats, whose functions have been extensively studied. Indeed, it is known that PKD repeats play established roles in protein–protein or protein–matrix interactions, mediating cell adhesion and cell-cell contact.

The variant c.11614G>A instead falls in the TOP domain[94], also called polycystin domain[95], which is shared with other polycystins. In PC-2, the TOP domain not only mediates homotypic interactions between PC-2 subunits, but also sits atop the voltage-sensing domain and the outer pore region, thus suggesting a role in channel gating [96]. Previous studies that aimed to dissect the formation of the PC complex have shown that PC-1 can interact with PC-2 in a 1:3 stoichiometry through coiled-coil domains present in their intracellular C-termini[97], and more recent evidence indicate that the S1–S2 extracellular loop

of PC-2 and the S6–S7 loop of PC-1 (corresponding to the TOP domain) play a crucial role in the assembly and function of the polycystin complex[98]. Unlike the TOP domain identified in PC-2, the PC-1 TOP domain lacks some of the interacting domains, thus excluding the possibility of PC-1 homodimerization[96]. In light of this, it is now clear that even a minor aminoacidic substitution in this domain can alter the stability of the PC complex, thus compromising its function as a Ca^{2+} permeable channel.

It is noteworthy to point out that a putative truncated form of PC-1 (around 200 kDa) was detected in our heterozygous and homozygous clones using an antibody raised against the N-terminal portion of the protein. This could be in line with the location of the DNA rupture on exon 15. However, we do not have any evidence whether this truncated form has a function or not, or whether it is delivered to the membrane exploiting at least its cell-cell and cell-matrix adhesion function. To do that, a first mass spectrometry analysis should be performed to verify whether the shorten form is indeed a product of the truncating variants introduced in exon 15. Secondly, proper functional assays should be carried out to discover its location in the cell (whether in membrane or internalized in the cytoplasm).

To sum up, our results showed that $Ex15^{+/-}/Ex42^{M/M}$ cells behave similarly to $Ex15^{-/-}$ concerning actin polymerization, focal adhesions' formation and autophagic pathway. Induced S/G_2 entry driven by Id2 induction was the only phenotype – among the ones we tested – that evidenced a difference between the two cell lines. Lastly, increased resistance to apoptosis seemed to be a shared phenotype also by the $Ex15^{+/+}/Ex42^{M/M}$ clones.

For FAs and consequent actin remodeling, we observed a similar pattern for both $Ex15^{-/-}$ and $Ex15^{+/-}/Ex42^{M/M}$ clones. This is reliable as previous work demonstrated the ability of PC-1 to bind the ECM and mediates cell-cell contacts through its N-terminal domain; not only, the C-terminal of the protein is instead involved in the phosphorylation of FAK and paxillin, stimulating the formation of FAs, clearly demonstrating that it has a pivotal role in mediating cell-adhesion[45].

Concerning proliferation and cell cycle, previous data demonstrated that, when PC-2 is phosphorylated on Serine 812, it is bound to Id2, retaining it in the cytoplasm and preventing its effect on p21 transcription leading to cell-cycle progression[99]. It is also known that this phosphorylation is PC-1 dependent. However, it is still not clear how this post-translational modification occurs: Serine812 is thought to be a putative phosphorylation site for Casein

Kinase 2 (CK2), and it was shown that in *Pkd1*$^{del34/del34}$ and *Pkd1*$^{null/null}$ mice, which do not have a functional PC-1, this residue is not phosphorylated and so Id2 is able to exert its function into the nucleus. Based on this and based on our results, we hypothesized that the variant on exon 42 does not affect the phosphorylation of PC-2, thus not impairing proliferation in Ex15$^{+/-}$/Ex42$^{M/M}$ as it does in Ex15$^{-/-}$ cells. To further prove this theory, we should verify the phosphorylation status of PC-2 in our clones[100].

Autophagy dysregulation has been lately described as one of the key features of ADPKD, but it is still controversial how the PC complex regulates this process. Several studies described a pivotal role in regulating macroautophagy both for PC-1 and PC-2. For instance, Peintner et al.[60] showed that *Pkd1*-deficient mouse inner medullary collecting duct cells (mIMCD3) and tubular epithelial cells isolated from nephrons of *pkd1* knockout mice showed diminished lysosomal acidification, LAMP degradation and reduced cathepsin B processing and activity. This led to an impairment of autophagosomal-lysosomal fusion, that happens because of an hyperactivation of Calpains (CAPNs), which are calcium-sensitive proteases. It is highly probable that the dysregulation of calcium influx plays a key role: *PKD1* could regulate calcium influx via its interaction partner *PKD2*, which operates as a cation channel that regulates calcium fluxes[101,102,103,19]. Coherently, Peña-Oyarzun et al.[61] demonstrated that *PKD2* have also an independent role in inducing autophagy, exploiting its ability to form complex with *BECN1*. The formation of this complex depends on the presence of the CC1 domain of *PKD2* and on intracellular Ca^{2+} mobilization. All together, these results suggest that the PC complex regulates autophagy through Ca^{2+}-dependent mechanisms. This may explain why our Ex15$^{-/-}$ and Ex15$^{+/-}$/Ex42$^{M/M}$ behave similarly, as both present mutations that affect either the formation or the stability of the PC complex.

Lastly, data concerning apoptosis are the only ones whose interpretation is still under debate. As a matter of fact, even though it has been previously demonstrated that cyst-lining cells (CD133+) are able to withstand apoptotic pathways better than their WT counterparts[52], general knowledge about the disease stated that actually apoptosis is massively induced in ADPKD, being one of the most important traits in polycystic kidneys[104,105,106]. Moreover, this is the only phenotype (among the ones tested) that do not highlight any differences between homozygous clones, including Ex15$^{+/+}$/Ex42$^{M/M}$.

A major limitation of this study is the selected cell line. HEK293T cells are not the most representative model to study ADPKD as they are not epithelial/renal-derived cell line,

lacking some of the typical morphological and functional traits of kidney-like cells (as RPTEC/hTERT1) and pose the problem of clonality. For instance, HEK293T are not cells able to grow tridimensionally on a layer of matrigel/collagen to form tubular[107] or cystic structures in case of mutations of PKD-related genes, which is the most evident phenotype characterizing the disease. However, the aim of this work is to create a library of cell lines bearing variants on *PKD1*, which normally is not prone to gene editing due to the high percentage of homology with its 6 pseudogenes. Moreover, for CRISPR/Cas9 to be effective in gene tagging, the technology must create a double-strand break (DSB) to induce NHEJ or homology-directed repair (HDR) in the case of knock-in mutants. Given that, all cells do not undergo HDR at the same efficiency and the ability to tag a given locus may vary between different cell lines. For instance, tubular-epithelial cell lines such as RPTEC/hTERT1 are conventionally not prone to be genetically modified for this reason[108], making them unsuitable to our aim. Anyhow, we demonstrated that HEK293T cells can recapitulate some of the "bidimensional" features of ADPKD, as several biological processes are altered similarly to what we can observed in patients' cystic cells. As concerning the clonality issue, we were able to overcome that by working with multiple clones carrying the variant on exon 42, but it remains a crucial point for those cell lines carrying the variants on exon 15. Indeed, the lower efficiency of the conventional CRISPR/Cas9 system led to the generation of a single clone both for the heterozygous and homozygous cells on exon 15, which will be solved generating and testing other clones to make sure that the selection process did not introduce any bias.

In conclusion, this work provides a starting point for the generation of different ADPKD-related variants, primarily in mutational hotspots (exons 15, 18, 23 and 46), using base editors and other cutting-edge genome editing approaches, such as prime editing and Cas9-RNP. The foremost goal is to create a library of cell lines carrying *PKD1* variants that can be studied in controlled experimental settings to determine their functional impact on the clinical phenotype. Moreover, one of the aims is to highlight differences based on the type of variants and location along the gene, complementing the already available knowledge about the genotype-phenotype correlations in ADPKD.

Acknowledgements

I would like to thank my mentors, Professors Silvia Deaglio and Tiziana Vaisitti for giving me the opportunity to get my Ph.D. in their laboratory, for devising this project, planning experiments, and critically interpreting results.

I would also like to thank the “lab gang”: you helped me to get more knowledge and technical skills. But that’s not just it. You taught me to not get upset when negative results come along the way but to embrace them as part of a long and exciting journey. You taught me how to organize experiments, how to critically read results, how to persistently think forward, while always enjoying the little things that happen in the present. Most of all, I learnt how life-changing is to communicate and to have a bond with people working around you, exchanging ideas and supporting each other.

I would also like to thank all the patients, clinicians, and colleagues for their participation in this project.

Thanks to my family and friends. Your presence eased the struggle when it was too overwhelming to see the silver lining. Thank you for being strong and positive when I was not. Thank you for always reminding me what is truly important and to always believe in me.

References

1. McEwan P, Bennett Wilton H, Ong ACM, et al. A model to predict disease progression in patients with autosomal dominant polycystic kidney disease (ADPKD): the ADPKD Outcomes Model. *BMC Nephrol*. 2018;19(1):37.
2. Harris PC, Torres VE. Polycystic kidney disease. *Annu Rev Med*. 2009;60:321-337.
3. Torres VE, Harris PC, Pirson Y. Autosomal dominant polycystic kidney disease. *Lancet*. 2007;369(9569):1287-1301.
4. Chapman AB, Devuyst O, Eckardt KU, et al. Autosomal-dominant polycystic kidney disease (ADPKD): executive summary from a Kidney Disease: Improving Global Outcomes (KDIGO) Controversies Conference. *Kidney Int*. 2015;88(1):17-27.
5. Cornec-Le Gall E, Audrezet MP, Chen JM, et al. Type of PKD1 mutation influences renal outcome in ADPKD. *J Am Soc Nephrol*. 2013;24(6):1006-1013.
6. Cornec-Le Gall E, Torres VE, Harris PC. Genetic Complexity of Autosomal Dominant Polycystic Kidney and Liver Diseases. *J Am Soc Nephrol*. 2018;29(1):13-23.
7. Heyer CM, Sundsbak JL, Abebe KZ, et al. Predicted Mutation Strength of Nontruncating PKD1 Mutations Aids Genotype-Phenotype Correlations in Autosomal Dominant Polycystic Kidney Disease. *J Am Soc Nephrol*. 2016;27(9):2872-2884.
8. Porath B, Gainullin VG, Cornec-Le Gall E, et al. Mutations in GANAB, Encoding the Glucosidase IIalpha Subunit, Cause Autosomal-Dominant Polycystic Kidney and Liver Disease. *Am J Hum Genet*. 2016;98(6):1193-1207.
9. Cornec-Le Gall E, Olson RJ, Besse W, et al. Monoallelic Mutations to DNAJB11 Cause Atypical Autosomal-Dominant Polycystic Kidney Disease. *Am J Hum Genet*. 2018;102(5):832-844.
10. Cornec-Le Gall E, Audrezet MP, Rousseau A, et al. The PROPKD Score: A New Algorithm to Predict Renal Survival in Autosomal Dominant Polycystic Kidney Disease. *J Am Soc Nephrol*. 2016;27(3):942-951.
11. Besse W, Choi J, Ahram D, et al. A noncoding variant in GANAB explains isolated polycystic liver disease (PCLD) in a large family. *Hum Mutat*. 2018;39(3):378-382.
12. https://pkdb.mayo.edu/welcome.
13. Shang S, Wang C, Chen L, et al. Novel method for the genomic analysis of PKD1 mutation in autosomal dominant polycystic kidney disease. *Front Cell Dev Biol*. 2022;10:937580.
14. Sampson JR, Maheshwar MM, Aspinwall R, et al. Renal cystic disease in tuberous sclerosis: role of the polycystic kidney disease 1 gene. *Am J Hum Genet*. 1997;61(4):843-851.
15. Huang S, Xu K, Xu Y, Zhao L, He X. TSC2/PKD1 contiguous deletion syndrome in a pregnant woman: A case report. *Front Med (Lausanne)*. 2023;10:1101079.
16. Bogdanova N, Markoff A, Gerke V, McCluskey M, Horst J, Dworniczak B. Homologues to the first gene for autosomal dominant polycystic kidney disease are pseudogenes. *Genomics*. 2001;74(3):333-341.
17. Bergmann C, Guay-Woodford LM, Harris PC, Horie S, Peters DJM, Torres VE. Polycystic kidney disease. *Nat Rev Dis Primers*. 2018;4(1):50.
18. Wilson PD. Polycystic kidney disease. *N Engl J Med*. 2004;350(2):151-164.
19. Su Q, Hu F, Ge X, et al. Structure of the human PKD1-PKD2 complex. *Science*. 2018;361(6406).
20. Ha K, Nobuhara M, Wang Q, et al. The heteromeric PC-1/PC-2 polycystin complex is activated by the PC-1 N-terminus. *Elife*. 2020;9.
21. Dong K, Miao H, Jia X, et al. Identification of a pathogenic mutation in a Chinese pedigree with polycystic kidney disease. *Mol Med Rep*. 2019;19(4):2671-2679.

22. Vien TN, Wang J, Ng LCT, Cao E, DeCaen PG. Molecular dysregulation of ciliary polycystin-2 channels caused by variants in the TOP domain. *Proc Natl Acad Sci U S A*. 2020;117(19):10329-10338.
23. Happe H, Leonhard WN, van der Wal A, et al. Toxic tubular injury in kidneys from Pkd1-deletion mice accelerates cystogenesis accompanied by dysregulated planar cell polarity and canonical Wnt signaling pathways. *Hum Mol Genet*. 2009;18(14):2532-2542.
24. Hwang YH, Conklin J, Chan W, et al. Refining Genotype-Phenotype Correlation in Autosomal Dominant Polycystic Kidney Disease. *J Am Soc Nephrol*. 2016;27(6):1861-1868.
25. Correction to "Incompletely penetrant PKD1 alleles suggest a role for gene dosage in cyst initiation in polycystic kidney disease". *Kidney Int*. 2009;75(12):1359.
26. Adzhubei IA, Schmidt S, Peshkin L, et al. A method and server for predicting damaging missense mutations. *Nat Methods*. 2010;7(4):248-249.
27. Choi Y, Sims GE, Murphy S, Miller JR, Chan AP. Predicting the functional effect of amino acid substitutions and indels. *PLoS One*. 2012;7(10):e46688.
28. Grantham JJ, Torres VE, Chapman AB, et al. Volume progression in polycystic kidney disease. *N Engl J Med*. 2006;354(20):2122-2130.
29. Cornec-Le Gall E, Audrezet MP, Renaudineau E, et al. PKD2-Related Autosomal Dominant Polycystic Kidney Disease: Prevalence, Clinical Presentation, Mutation Spectrum, and Prognosis. *Am J Kidney Dis*. 2017;70(4):476-485.
30. Vujic M, Heyer CM, Ars E, et al. Incompletely penetrant PKD1 alleles mimic the renal manifestations of ARPKD. *J Am Soc Nephrol*. 2010;21(7):1097-1102.
31. Rossetti S, Kubly VJ, Consugar MB, et al. Incompletely penetrant PKD1 alleles suggest a role for gene dosage in cyst initiation in polycystic kidney disease. *Kidney Int*. 2009;75(8):848-855.
32. Losekoot M, Ruivenkamp CA, Tholens AP, et al. Neonatal onset autosomal dominant polycystic kidney disease (ADPKD) in a patient homozygous for a PKD2 missense mutation due to uniparental disomy. *J Med Genet*. 2012;49(1):37-40.
33. Y Pei ADP, K R Wang, N He, D Hefferton, T Watnick, G G Germino, P Parfrey, S Somlo, P St George-Hyslop. Bilineal Disease and Trans-Heterozygotes in Autosomal Dominant Polycystic Kidney Disease. *The American Journal of Human Genetic*. 2001.
34. Izzi C, Dordoni C, Delbarba E, et al. Lessons From the Clinic: ADPKD Genetic Test Unraveling Severe Phenotype, Intrafamilial Variability, and New, Rare Causing Genotype. *Kidney Int Rep*. 2022;7(4):895-898.
35. Graziani L, Zampatti S, Carriero ML, et al. Co-Inheritance of Pathogenic Variants in PKD1 and PKD2 Genes Determined by Parental Segregation and De Novo Origin: A Case Report. *Genes (Basel)*. 2023;14(8).
36. Sekine A, Hoshino J, Fujimaru T, et al. Genetics May Predict Effectiveness of Tolvaptan in Autosomal Dominant Polycystic Kidney Disease. *Am J Nephrol*. 2020;51(9):745-751.
37. Zhang Z, Bai H, Blumenfeld J, et al. Detection of PKD1 and PKD2 Somatic Variants in Autosomal Dominant Polycystic Kidney Cyst Epithelial Cells by Whole-Genome Sequencing. *J Am Soc Nephrol*. 2021;32(12):3114-3129.
38. Watnick T, He N, Wang K, et al. Mutations of PKD1 in ADPKD2 cysts suggest a pathogenic effect of trans-heterozygous mutations. *Nat Genet*. 2000;25(2):143-144.
39. Torres VE, Harris PC. Autosomal dominant polycystic kidney disease: the last 3 years. *Kidney Int*. 2009;76(2):149-168.
40. Wilson PD. Polycystin: new aspects of structure, function, and regulation. *J Am Soc Nephrol*. 2001;12(4):834-845.
41. Roitbak T, Ward CJ, Harris PC, Bacallao R, Ness SA, Wandinger-Ness A. A polycystin-1 multiprotein complex is disrupted in polycystic kidney disease cells. *Mol Biol Cell*. 2004;15(3):1334-1346.

42. Streets AJ, Prosseda PP, Ong AC. Polycystin-1 regulates ARHGAP35-dependent centrosomal RhoA activation and ROCK signaling. *JCI Insight*. 2020;5(16).
43. Geng L, Burrow CR, Li HP, Wilson PD. Modification of the composition of polycystin-1 multiprotein complexes by calcium and tyrosine phosphorylation. *Biochim Biophys Acta*. 2000;1535(1):21-35.
44. Castelli M, De Pascalis C, Distefano G, et al. Regulation of the microtubular cytoskeleton by Polycystin-1 favors focal adhesions turnover to modulate cell adhesion and migration. *BMC Cell Biol*. 2015;16:15.
45. Joly D, Ishibe S, Nickel C, Yu Z, Somlo S, Cantley LG. The polycystin 1-C-terminal fragment stimulates ERK-dependent spreading of renal epithelial cells. *J Biol Chem*. 2006;281(36):26329-26339.
46. Woo D. Apoptosis and loss of renal tissue in polycystic kidney diseases. *N Engl J Med*. 1995;333(1):18-25.
47. Veis DJ, Sorenson CM, Shutter JR, Korsmeyer SJ. Bcl-2-deficient mice demonstrate fulminant lymphoid apoptosis, polycystic kidneys, and hypopigmented hair. *Cell*. 1993;75(2):229-240.
48. Moser M, Pscherer A, Roth C, et al. Enhanced apoptotic cell death of renal epithelial cells in mice lacking transcription factor AP-2beta. *Genes Dev*. 1997;11(15):1938-1948.
49. Lin HH, Yang TP, Jiang ST, Yang HY, Tang MJ. Bcl-2 overexpression prevents apoptosis-induced Madin-Darby canine kidney simple epithelial cyst formation. *Kidney Int*. 1999;55(1):168-178.
50. Boletta A, Qian F, Onuchic LF, et al. Polycystin-1, the gene product of PKD1, induces resistance to apoptosis and spontaneous tubulogenesis in MDCK cells. *Mol Cell*. 2000;6(5):1267-1273.
51. Nowak KL, Edelstein CL. Apoptosis and autophagy in polycystic kidney disease (PKD). *Cell Signal*. 2020;68:109518.
52. Carvalhosa R, Deambrosis I, Carrera P, et al. Cystogenic potential of CD133+ progenitor cells of human polycystic kidneys. *J Pathol*. 2011;225(1):129-141.
53. Boletta A. Emerging evidence of a link between the polycystins and the mTOR pathways. *Pathogenetics*. 2009;2(1):6.
54. Shillingford JM, Murcia NS, Larson CH, et al. The mTOR pathway is regulated by polycystin-1, and its inhibition reverses renal cystogenesis in polycystic kidney disease. *Proc Natl Acad Sci U S A*. 2006;103(14):5466-5471.
55. Shillingford JM, Piontek KB, Germino GG, Weimbs T. Rapamycin ameliorates PKD resulting from conditional inactivation of Pkd1. *J Am Soc Nephrol*. 2010;21(3):489-497.
56. Nadasdy T, Laszik Z, Lajoie G, Blick KE, Wheeler DE, Silva FG. Proliferative activity of cyst epithelium in human renal cystic diseases. *J Am Soc Nephrol*. 1995;5(7):1462-1468.
57. Cabrita I, Kraus A, Scholz JK, et al. Cyst growth in ADPKD is prevented by pharmacological and genetic inhibition of TMEM16A in vivo. *Nat Commun*. 2020;11(1):4320.
58. Li X. Polycystin-1 and polycystin-2 regulate the cell cycle through the helix–loop–helix inhibitor Id2. *nature cell biology*. 2005.
59. Mizushima N. Autophagy: process and function. *Genes Dev*. 2007;21(22):2861-2873.
60. Peintner L, Venkatraman A, Waeldin A, et al. Loss of PKD1/polycystin-1 impairs lysosomal activity in a CAPN (calpain)-dependent manner. *Autophagy*. 2021;17(9):2384-2400.
61. Pena-Oyarzun D, Rodriguez-Pena M, Burgos-Bravo F, et al. PKD2/polycystin-2 induces autophagy by forming a complex with BECN1. *Autophagy*. 2021;17(7):1714-1728.
62. Criollo A, Altamirano F, Pedrozo Z, et al. Polycystin-2-dependent control of cardiomyocyte autophagy. *J Mol Cell Cardiol*. 2018;118:110-121.
63. Pampliega O, Orhon I, Patel B, et al. Functional interaction between autophagy and ciliogenesis. *Nature*. 2013;502(7470):194-200.

64. Wang S, Livingston MJ, Su Y, Dong Z. Reciprocal regulation of cilia and autophagy via the MTOR and proteasome pathways. *Autophagy*. 2015;11(4):607-616.
65. Tran Nguyen Truc L, Matsuda S, Takenouchi A, et al. Mechanism of cystogenesis by Cd79a-driven, conditional mTOR activation in developing mouse nephrons. *Sci Rep*. 2023;13(1):508.
66. Holditch SJ, Brown CN, Atwood DJ, et al. A study of sirolimus and mTOR kinase inhibitor in a hypomorphic Pkd1 mouse model of autosomal dominant polycystic kidney disease. *Am J Physiol Renal Physiol*. 2019;317(1):F187-F196.
67. Stayner C, Shields J, Slobbe L, Shillingford JM, Weimbs T, Eccles MR. Rapamycin-mediated suppression of renal cyst expansion in del34 Pkd1-/- mutant mouse embryos: an investigation of the feasibility of renal cyst prevention in the foetus. *Nephrology (Carlton)*. 2012;17(8):739-747.
68. Li A, Fan S, Xu Y, et al. Rapamycin treatment dose-dependently improves the cystic kidney in a new ADPKD mouse model via the mTORC1 and cell-cycle-associated CDK1/cyclin axis. *J Cell Mol Med*. 2017;21(8):1619-1635.
69. Tanaka Y, Watari M, Saito T, Morishita Y, Ishibashi K. Enhanced Autophagy in Polycystic Kidneys of AQP11 Null Mice. *Int J Mol Sci*. 2016;17(12).
70. Zehender A, Li YN, Lin NY, et al. TGFbeta promotes fibrosis by MYST1-dependent epigenetic regulation of autophagy. *Nat Commun*. 2021;12(1):4404.
71. Ponticelli C, Moroni G, Reggiani F. Autosomal Dominant Polycystic Kidney Disease: Is There a Role for Autophagy? *Int J Mol Sci*. 2023;24(19).
72. Kuraoka S, Tanigawa S, Taguchi A, et al. PKD1-Dependent Renal Cystogenesis in Human Induced Pluripotent Stem Cell-Derived Ureteric Bud/Collecting Duct Organoids. *J Am Soc Nephrol*. 2020;31(10):2355-2371.
73. Tan YC, Michaeel A, Blumenfeld J, et al. A novel long-range PCR sequencing method for genetic analysis of the entire PKD1 gene. *J Mol Diagn*. 2012;14(4):305-313.
74. Iannello A, Vitale N, Coma S, et al. Synergistic efficacy of the dual PI3K-delta/gamma inhibitor duvelisib with the Bcl-2 inhibitor venetoclax in Richter syndrome PDX models. *Blood*. 2021;137(24):3378-3389.
75. Tang Z, Lin MG, Stowe TR, et al. Autophagy promotes primary ciliogenesis by removing OFD1 from centriolar satellites. *Nature*. 2013;502(7470):254-257.
76. Yang N, Higuchi O, Ohashi K, et al. Cofilin phosphorylation by LIM-kinase 1 and its role in Rac-mediated actin reorganization. *Nature*. 1998;393(6687):809-812.
77. Hsu GC, Wang Y, Lu AZ, et al. TIAM1 acts as an actin organization regulator to control adipose tissue-derived pericyte cell fate. *JCI Insight*. 2023;8(13).
78. Sindram E, Caballero-Oteyza A, Kogata N, et al. ARPC5 deficiency leads to severe early-onset systemic inflammation and mortality. *Dis Model Mech*. 2023;16(7).
79. Zhang Y, Reif G, Wallace DP. Extracellular matrix, integrins, and focal adhesion signaling in polycystic kidney disease. *Cell Signal*. 2020;72:109646.
80. Mitra SK, Hanson DA, Schlaepfer DD. Focal adhesion kinase: in command and control of cell motility. *Nat Rev Mol Cell Biol*. 2005;6(1):56-68.
81. Chiu YW, Liou LY, Chen PT, et al. Tyrosine 397 phosphorylation is critical for FAK-promoted Rac1 activation and invasive properties in oral squamous cell carcinoma cells. *Lab Invest*. 2016;96(3):296-306.
82. Julie X. Zhou LXF, Xiaoyan Li,James P. Calvet,Xiaogang Li. TNFα Signaling Regulates Cystic Epithelial Cell Proliferation through Akt/mTOR and ERK/MAPK/Cdk2 Mediated Id2 Signaling. *PLoS One*. 2015.
83. Fan LX, Li X, Magenheimer B, Calvet JP, Li X. Inhibition of histone deacetylases targets the transcription regulator Id2 to attenuate cystic epithelial cell proliferation. *Kidney Int*. 2012;81(1):76-85.

84. Hughes P, Robati M, Lu W, Zhou J, Strasser A, Bouillet P. Loss of PKD1 and loss of Bcl-2 elicit polycystic kidney disease through distinct mechanisms. *Cell Death Differ*. 2006;13(7):1123-1127.
85. Zhu P, Sieben CJ, Xu X, Harris PC, Lin X. Autophagy activators suppress cystogenesis in an autosomal dominant polycystic kidney disease model. *Hum Mol Genet*. 2017;26(1):158-172.
86. Wang S, Dong Z. Is autophagy the culprit of cystogenesis in polycystic kidney disease? *EBioMedicine*. 2020;61:103043.
87. Ravichandran K, Edelstein CL. Polycystic kidney disease: a case of suppressed autophagy? *Semin Nephrol*. 2014;34(1):27-33.
88. Geetha T, Wooten MW. Association of the atypical protein kinase C-interacting protein p62/ZIP with nerve growth factor receptor TrkA regulates receptor trafficking and Erk5 signaling. *J Biol Chem*. 2003;278(7):4730-4739.
89. Pankiv S, Clausen TH, Lamark T, et al. p62/SQSTM1 binds directly to Atg8/LC3 to facilitate degradation of ubiquitinated protein aggregates by autophagy. *J Biol Chem*. 2007;282(33):24131-24145.
90. Yuan Xue SP, Jing Xie, Dinah Clark, Fang Fang eP418: Enabling reclassification of missense variants in PKD1/2 – the power of a commercial laboratory database. *Genetics in Medicine*. 2022;24(3):S262.
91. Benz EG, Hartung EA. Correction to: "Predictors of progression in autosomal dominant and autosomal recessive polycystic kidney disease". *Pediatr Nephrol*. 2021;36(9):2895-2897.
92. Kamura M, Yamamura T, Omachi K, et al. Trimerization and Genotype-Phenotype Correlation of COL4A5 Mutants in Alport Syndrome. *Kidney Int Rep*. 2020;5(5):718-726.
93. Rees HA, Liu DR. Publisher Correction: Base editing: precision chemistry on the genome and transcriptome of living cells. *Nat Rev Genet*. 2018;19(12):801.
94. Grieben M, Pike AC, Shintre CA, et al. Structure of the polycystic kidney disease TRP channel Polycystin-2 (PC2). *Nat Struct Mol Biol*. 2017;24(2):114-122.
95. Shen PS, Yang X, DeCaen PG, et al. The Structure of the Polycystic Kidney Disease Channel PKD2 in Lipid Nanodiscs. *Cell*. 2016;167(3):763-773 e711.
96. Padovano V, Caplan MJ. The Polycystin Complex Reveals Its Complexity. *Biochemistry*. 2018;57(51):6917-6918.
97. Yu Y, Ulbrich MH, Li MH, et al. Structural and molecular basis of the assembly of the TRPP2/PKD1 complex. *Proc Natl Acad Sci U S A*. 2009;106(28):11558-11563.
98. Salehi-Najafabadi Z, Li B, Valentino V, et al. Extracellular Loops Are Essential for the Assembly and Function of Polycystin Receptor-Ion Channel Complexes. *J Biol Chem*. 2017;292(10):4210-4221.
99. Streets A, Ong A. Post-translational modifications of the polycystin proteins. *Cell Signal*. 2020;72:109644.
100. Cai Y, Anyatonwu G, Okuhara D, et al. Calcium dependence of polycystin-2 channel activity is modulated by phosphorylation at Ser812. *J Biol Chem*. 2004;279(19):19987-19995.
101. Fedeles SV, Gallagher AR, Somlo S. Polycystin-1: a master regulator of intersecting cystic pathways. *Trends Mol Med*. 2014;20(5):251-260.
102. Nauli SM, Alenghat FJ, Luo Y, et al. Polycystins 1 and 2 mediate mechanosensation in the primary cilium of kidney cells. *Nat Genet*. 2003;33(2):129-137.
103. Busch T, Kottgen M, Hofherr A. TRPP2 ion channels: Critical regulators of organ morphogenesis in health and disease. *Cell Calcium*. 2017;66:25-32.
104. Nowak KL, Edelstein CL. Apoptosis and autophagy in polycystic kidney disease (PKD). *Cellular Signalling*. 2020;68.

105. Peintner L, Borner C. Role of apoptosis in the development of autosomal dominant polycystic kidney disease (ADPKD). *Cell Tissue Res*. 2017;369(1):27-39.
106. Agborbesong E, Li LX, Li L, Li X. Molecular Mechanisms of Epigenetic Regulation, Inflammation, and Cell Death in ADPKD. *Front Mol Biosci*. 2022;9:922428.
107. Secker PF, Luks L, Schlichenmaier N, Dietrich DR. RPTEC/TERT1 cells form highly differentiated tubules when cultured in a 3D matrix. *ALTEX*. 2018;35(2):223-234.
108. Veach RA, Wilson MH. CRISPR/Cas9 engineering of a KIM-1 reporter human proximal tubule cell line. *PLoS One*. 2018;13(9):e0204487.
109. Ferreira FM, Watanabe EH, Onuchic LF. Polycystins and Molecular Basis of Autosomal Dominant Polycystic Kidney Disease. In: Li X, ed. Polycystic Kidney Disease. Brisbane (AU); 2015.

Tables

Table 1. sgRNA design and CRISPR/Cas9 plasmid used to introduce the variants of interest.

sgRNA name	Sequence	CRISPR/Cas9 system
EXON15	GCTCCTCCAACACGACCGTGCGG	pCW-Cas9
EXON42	GAACTCGAGGCGCAGCGTGACGG	pCMV-AncBE4max-P2A-GFP

Table 2. LR-PCR primers used to amplify PKD1 gene.

Fragment	Size (bp)	Exon	Forward primer (5'-3')	Reverse primer (5'-3')
Gene 13-15	4391	13-15	TGGAGGGAGGGACGCCAATC	GTCAACGTGGGCCTCCAAGT
Gene 42-46	2370	42-46	GAGTAGTTCTCCAGGAGTGCCG	ATTCTGCCTGGCCCTCGGCCTT

Table 3. Nested and sequecing primers used for exon 15 and exon 42.

Primer name	Forward primer (5'-3')	Reverse primer (5'-3')	Exons covered
PKD1-exon15B	GACATGAGCCTGGCCGTGG	CCACCTCTGGCTCCACGCA	15
PKD1-exon42	CCTCAGCCACGCCTGCACT	GGGTGAGACGCTGCCGGG	42

Table 4. List of primary antibodies used.

Target	Application	Company	Product ID
p-FAK (Tyr397)	IF	Cell Signaling Technologies	8556
Id2	WB	Cell Signaling Technologies	3431
LC3B	WB	Cell Signaling Technologies	2775
Polycystin-1 (7E12)	WB	Santa Cruz	sc-130554
beta-actin (13E5)	WB	Cell Signaling Technologies	5125
Pan-ERK	WB	BD Biosciences	610124
alpha-tubulin	WB	Cell Signaling Technologies	2144
Lamin A/C	WB	Cell Signaling Technologies	2032

IF: Immunofluorescence

WB: Western Blot

Table 5. List of genes belonging to up-regulated GO terms

	Term	P.value	Genes	Sample
BASAL	Epithelial Mesenchymal Transition	4.4E-04	SFRP1;CDH2;LAMA3;CD44	Ex15$^{+/-}$
	Epithelial Mesenchymal Transition	9.0E-05	SFRP1;COL12A1;FN1;SDC1;CRLF1;FBN1	Ex15$^{-/-}$
	p53 Pathway	6.2E-03	PROCR;BMP2;SDC1;NDRG1	
	TGF-beta Signaling	1.7E-02	BMP2;SMAD6	
	KRAS Signaling Up	3.7E-02	BMP2;MAFB;ALDH1A2	
	G2-M Checkpoint	2.2E-06	HSPA8;CENPE;SQLE;CENPF;MKI67	Ex15$^{+/+}$/Ex42^{MM}
	Mitotic Spindle	2.0E-02	CENPE;CENPF	
	E2F Targets	2.0E-02	CENPE;MKI67	
	Mitotic Spindle	1.6E-09	PIF1;NUMA1;ITSN1;NDC80;CENPE;CCNB2;CENPF;NIN;PRC1;CNTRL;FSCN1;CEP250;MYH9;SPTAN1;BUB1;DLGAP5	Ex15$^{+/-}$/Ex42^{MM}
	G2-M Checkpoint	6.7E-07	HSPA8;NUMA1;KNL1;HMMR;MKI67;NDC80;CENPE;CCNB2;CENPF;PTTG1;PRC1;STMN1;BUB1	
	Epithelial Mesenchymal Transition	9.2E-03	ACTA2;TPM4;COL4A2;COL5A1;COL4A1;COL6A2;DPYSL3	
STARVING	Epithelial Mesenchymal Transition	4.1E-03	SFRP1;BASP1;COL5A2;LAMA3;FN1;EDIL3;CD44	Ex15$^{+/-}$
	Apical Surface	9.7E-03	SCUBE1;CROCC;GATA3	Ex15$^{-/-}$
	Epithelial Mesenchymal Transition	2.3E-08	CXCL8;COL12A1;APLP1;TFPI2;FN1;NID2;FBLN2;LOXL2;COL1A1;SFRP1;COL3A1;BASP1;SDC1;PTX3;CRLF1;FBN1	
	TGF-beta Signaling	1.0E-04	BMP2;NOG;ID1;ID3;SMAD6;SMAD7	
	Apical Junction	2.2E-02	MAP4K2;ITGB4;CNTN1;SHROOM2;NRXN2;ICAM1;FBN1	
	p53 Pathway	2.2E-02	BMP2;ITGB4;GLS2;PLK2;FDXR;SDC1;FGF13	
	Apical Surface	2.3E-02	SCUBE1;SHROOM2;GATA3	
	Epithelial Mesenchymal Transition	9.3E-03	ACTA2;COL3A1;APLP1;HTRA1	Ex15$^{+/-}$/Ex42^{MM}

Table 6. List of genes belonging to down-regulated GO terms

	Term	P.value	Genes	Sample
BASAL	mTORC1 Signaling	-5.2E-04	SLC7A5;CTH;DDIT4;SLC7A11;NUPR1	Ex15$^{-/-}$
	p53 Pathway	-2.8E-02	DDIT4;SLC7A11;NUPR1	
	Reactive Oxygen Species Pathway	-1.2E-03	FES;MGST1;MBP	Ex15$^{+/+}$/Ex42$^{M/M}$
	TNF-alpha Signaling via NF-kB	-1.5E-10	KLF10;PPP1R15A;EGR1;CEBPB;EGR3;GADD45B;DUSP1;TNC;FOS;EIF1;RELB;VEGFA;NFKB	Ex15$^{+/-}$/Ex42$^{M/M}$
	p53 Pathway	-2.0E-04	PPP1R15A;CSRNP2;TRAF4;DDIT4;TRIB3;SLC3A2;SLC7A11;FOS;TRIAP1;ATF3;IER3	
	mTORC1 Signaling	-3.0E-03	PPP1R15A;SLC7A5;XBP1;CTH;DDIT4;TRIB3;SLC1A4;SLC7A11;BCAT1	
	TGF-beta Signaling	-8.2E-03	KLF10;PPP1R15A;ID2;ID1	
	Apoptosis	-1.0E-02	EGR3;GADD45B;CTH;RARA;ATF3;IER3;BCL2L1	
STARVING	KRAS Signaling Up	-1.7E-06	GUCY1A1;TMEM158;MAFB;CA2;IGFBP3;CXCR4;TNFAIP3;PLAT;TRIB1;PTGS2;ETV4;ETV5	Ex15$^{+/-}$
	Epithelial Mesenchymal Transition	-5.9E-05	TGFB1;CXCL8;GADD45B;LOX;IGFBP3;TNC;TIMP3;TNFAIP3;THBS1;GEM	
	TGF-beta Signaling	-2.6E-03	KLF10;TGFB1;JUNB;THBS1	
	Apoptosis	-2.9E-02	CCNA1;GADD45B;TIMP3;PLAT;IER3	
	Epithelial Mesenchymal Transition	-2.0E-04	TNFRSF12A;CDH2;IGFBP3;COL5A3;COL7A1;TNC;LAMC2;INHBA;CD44	Ex15$^{-/-}$
	Apoptosis	-6.0E-03	EGR3;ANXA1;TNFRSF12A;PEA15;PSEN2;CD44	
	KRAS Signaling Up	-1.6E-02	IGFBP3;GABRA3;INHBA;NGF;MMP10;MPZL2	
	Epithelial Mesenchymal Transition	-3.3E-03	CXCL8;ADAM12;TFPI2;LAMA3;FBN1	Ex15+/+/Ex42$^{M/M}$
	p53 Pathway	-3.3E-03	VAMP8;DDIT3;PDGFA;FGF13;ATF3	
	TNF-alpha Signaling via NF-kB7	-1.8E-02	TNFRSF9;SLC2A3;PTGS2;ATF3	
	Apoptosis	-4.7E-02	LGALS3;DDIT3;ATF3	
	TNF-alpha Signaling via NF-kB	-9.1E-06	KLF6;DUSP1;MYC;MAFF;TNC;GEM	Ex15+/-/Ex42$^{M/M}$
	Myc Targets V1	-1.4E-03	PSMB3;C1QBP;MYC;RPL6	
	Epithelial Mesenchymal Transition	-1.4E-03	SPARC;CDH2;TNC;GEM	

Figure Legend

Figure 1. Schematic representation of the *PKD1* mutant clones' generation

(A) HEK293T cells were transfected with either an empty vector or a sgRNA targeting exon 15 of *PKD1* to generate homozygous and heterozygous clones using a conventional CRISPR/Cas9 approach. Then, $Ex15^{+/+}$ and $Ex15^{+/-}$ clones were used to introduce an additional variant c.11614G>A;p.E3872K, using cytosine base editor (CBE) and only homozygous clones were selected.

(B) Truncating mutations on exon 15 target an important extracellular domain of the protein, called PKD repeats that share sequence similarity with immunoglobulin-like and fibronectin type-3 domains[109]. The missense variant introduces an aminoacidic change in one of the transmembrane domains (TM) potentially important for the stability of the protein and its interaction with PC-2.

(C) Representation of PC complex with a particular focus on the mutation site of c.11614G>A;p.E3872K. PC-1 is depicted in cyan and PC-2 in grey. The substitution of the glutamate into a lysine should induce a disruption of a hydrogen bond that links the oxygen of the carboxylic group of the glutamate to the amminic group of the backbone (dashed yellow line), resulting in a structural destabilization of PC-1. Images generated by the lab of Professor Dell'Orco (University of Verona).

Figure 2. *PKD1* transcript and PC-1 protein levels confirm the genetics of the generated clones

(A) Chromatograms obtained from Sanger sequencing of all the *PKD1* WT and mutant clones. Exons 15 and 42 were both amplified through a Long-Range PCR using primers previously validated by[73]. A second amplification was performed using internal primers.

(B) Transcript level of *PKD1* was evaluated in all clones through RT-PCR (at least $n = 5$) using a pair of primers that amplify exon 33 of the gene[52].

(C) Western blot for Polycystin-1. $Ex15^{+/+}$ and $Ex15^{+/+}/Ex42^{M/M}$ present full-length (FL) PC-1 protein (460 kDa), while $Ex15^{+/-}$ and $Ex15^{+/-}/Ex42^{M/M}$ present half of the amount of the FL form and a putative truncated protein (CL) around 120 kDa, generated by the interruption of translation in exon 15. Consequently, full knock-out $Ex15^{-/-}$ did not show FL PC-1 but only the truncated form.

Figure 3. Unsupervised analyses highlight a different clusterization between basal and starving conditions ad among clones with different genetics

(A) PCA analyses of variance-stabilized transformed (vst) counts of the five different clones, either cultured in complete (basal) or serum-deprived medium (starving). The first 2 components, which respectively accounted for the 24% and the 16.9% of the variance among all clones, were plotted. The two replicates of each clone used to perform the subsequent bioinformatic analyses are depicted. The dashed line was manually drawn to highlight the two different clusters (basal and starving).

Figure 4. DEG and GO analyses reveal dysregulation of terms related to ADPKD both in $Ex15^{-/-}$ and $Ex15^{+/-}/Ex42^{M/M}$

(A,B) Upset plots of DEG identified in all clones compared to the control ($Ex15^{+/+}$) cultured in basal (A) and starving (B) condition. Upper panel (red) represent upregulated genes, whilst the lower panel (blue) the down-regulated ones. Set size indicates the total number of genes in a given set, whereas intersection size indicates the number of genes that are in common amongst the comparisons, or unique to each set.

(C,D) GO analyses performed on DEG identified in all clones compared to the control ($Ex15^{+/+}$) underlining terms up- or down- regulated in basal (C) and in starving (D) culturing condition. Size of the dots correlates with the number of genes comprised in each term. Genes associated to each term are listed in table 5 and table 6. Statistical significance of each term is expressed as -log10(pvalue).

Figure 5. Differential expressed genes underline pathway-specific differences among clones

Heatmaps of genes associated to specific GO terms – normally dysregulated in ADPKD – such as cytoskeleton (A), cell- and focal adhesion (B), cell cycle (C) and autophagy (D).

Figure 6. Ex15$^{-/-}$ and Ex15$^{+/-}$/Ex42$^{M/M}$ clones show defective actin polymerization and disrupted formation of focal adhesions

(A) Immunostaining of F-actin (Phd - red) and nuclei (DAPI - blue) of the five cell lines to highlight potential defect in actin polymerization and cell adhesion. The number of actin filaments were then manually counted using ImageJ (at least *n = 4*). Each dot represents one cell. Error bars represents Standard Deviation (SD). Statistical analysis was performed using un-paired parametric t test.

(B) Immunostaining of phospho-FAK (Y397) (pFAK – green), actin (phalloidin - red) and nuclei (DAPI – blue) of the five cell lines previously starved over-night and then plated on fibronectin-treated coverslip for 1 hour. Ex15$^{+/+}$, Ex15$^{+/-}$, Ex15$^{+/+}$/Ex42$^{M/M}$ preserve the ability to properly form FAs (accumulation of active FAK), while Ex15$^{-/-}$ and Ex15$^{+/-}$/Ex42$^{M/M}$ present less activated FAK mainly localized at cytoplasmic level (at least *n = 3*).

Figure 7. In a serum-deprived condition, Ex15$^{-/-}$ clone enters in S/G$_2$ phases more easily than other clones due to the induction of Id2

(A) A schematic representation of the pathway that connects PC proteins and inhibitor od differentiation 2 (Id2) in regulating cystic epithelial cell proliferation (revised from [83]). Loss of *PKD1* results in the upregulation of Id2 and it affects indirectly also the shuttling of Id2 between nuclear and cytosolic compartments.

(B) Cell-cycle analysis was performed after 48h in basal and starving culture condition. Asterisks indicate statistical significance calculated against Ex15$^{+/+}$.

(C) RT-PCR and whole-cell lysate western blot performed after 48h (at least *n = 6*) to evaluate the transcription of *ID2* and production of its protein. Black asterisks indicate statistical significance calculated against Ex15$^{+/+}$. Red asterisks indicate statistical significance calculated considering the same clone in the two culturing conditions.

(D) Level of Id2 in Cytoplasmic-Nuclear fractions both in basal and in starving conditions. Lamin A/C (74 and 65 kDa) is used as a nuclear marker, while a-tubulin (52 kDa) as a cytoplasmic marker. Actin was used to normalize Id2 expression. Black asterisks indicate statistical significance calculated against Ex15$^{+/+}$. Red asterisks indicate statistical significance calculated considering the same clone in the two culturing conditions (experiments were performed at least five times).

Error bars represents Standard Deviation (SD). Statistical analysis was performed using un-paired parametric t test.

Figure 8. All homozygous clones ($Ex15^{-/-}$, $Ex15^{+/+}/Ex42^{M/M}$ and $Ex15^{+/-}/Ex42^{M/M}$) show an increased resistance to apoptosis in a stressful environment

(A) Cytofluorimetric profiles of necrotic (Q1), late-apoptotic (Q2), live (Q3) and early apoptotic (Q4) cells after Annexin-V/PI staining. Analysis of apoptosis rate was performed after 68h of starving.

(B) Cumulative graph of at least *n = 6* experiments showing the percentage of live cells in basal or in starving medium after 68h.
Error bars represents Standard Deviation (SD). Statistical analysis was performed using un-paired parametric t test.

Figure 9. $Ex15^{-/-}$ and compound heterozygous clones fail to convert LC3BI to LC3BII suggesting a potential defective autophagic flux

(A) Quantification of LC3B conversion from isoform I (17 kDa) to isoform II (14 kDa) assessed by western blot in cells cultured in complete medium (basal) or in serum-deprived medium (starving for 48h) either un-treated or treated with choloroquine (CQ) [100uM] for five hours, a drug whose mechanism of action is to block the binding of autophagosomes to lysosomes by altering the acidic environment of lysosomes (at least *n = 3*). Actin was used as a normalizing protein.

(B) Autophagic flux was better dissected using the Premo Autophagy kit, based on the infection of cells with a construct containing LC3B cDNA, associated with an acidic-sensitive GFP and an acidic-insensitive RFP. As depicted in the graphical representation of how the system works, infected cells start to transcribe and translate the entire construct. If LC3B-GFP-RFP localize on the autophagosomes' membrane, the two colors are maintained, and yellow dots are visible (autophagosomes). When autophagosomes fuse with lysosomes, the acidic environment causes the release of the GFP marker, thus leading to the formation of red dots (autolysosomes). Cells were infected simultaneously with plating on poly-L-lysine treated coverslips. After 16h, medium was changes and serum-deprived medium was added. After 24h, we proceed with fixing and staining with DAPI.

Analysis was conducted with ImageJ and at least 6 images per experiment (*n = 5*) were analyzed. Manders coefficient (M2) was plotted to highlight the fraction of red signal co-localizing with green signal (the closer is to 1 the more is colocalizing). Error bars represents Standard Deviation (SD). Statistical analysis was performed using un-paired parametric t test.

Figures

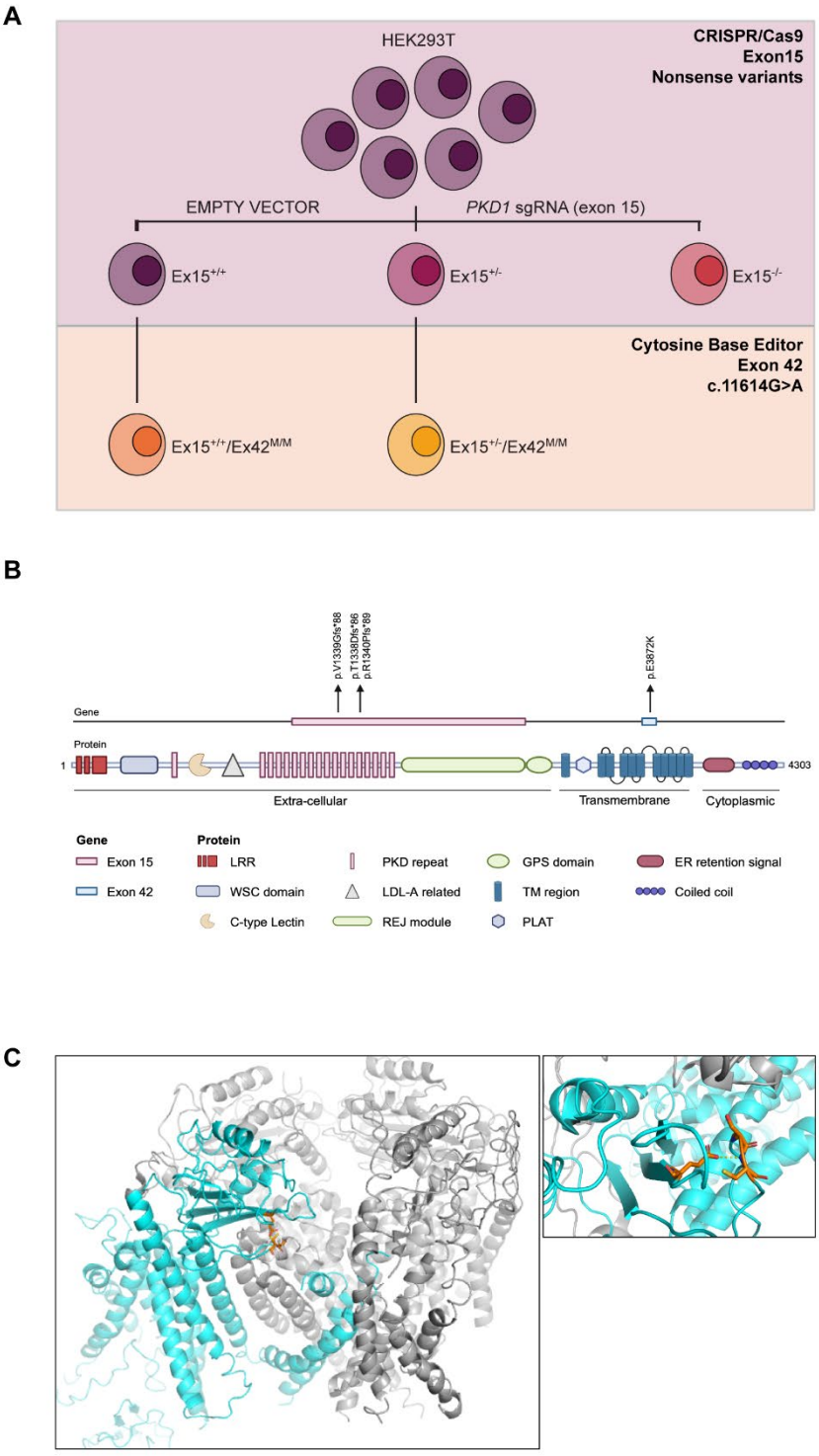

Figure 1

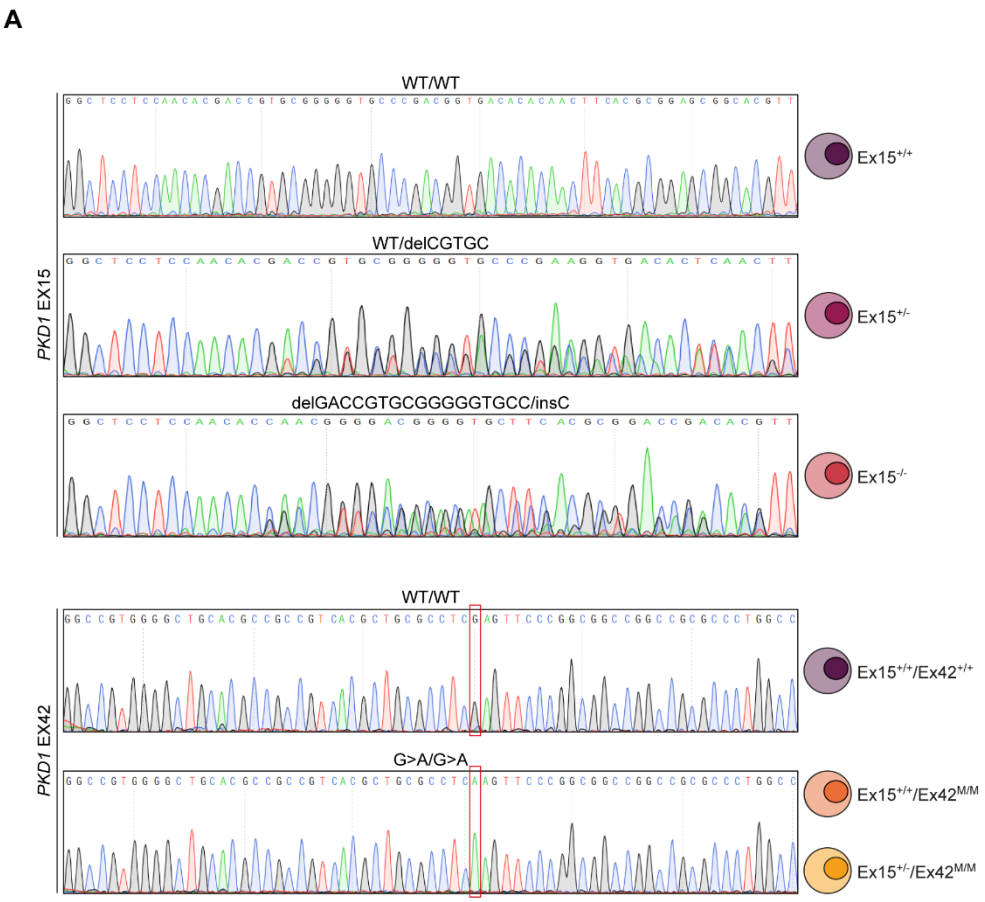
A
WT/WT
WT/delCGTGC
delGACCGTGCGGGGGTGCC/insC
PKD1 EX15
Ex15+/+
Ex15+/-
Ex15-/-
WT/WT
G>A/G>A
PKD1 EX42
Ex15+/+/Ex42+/+
Ex15+/+/Ex42M/M
Ex15+/-/Ex42M/M

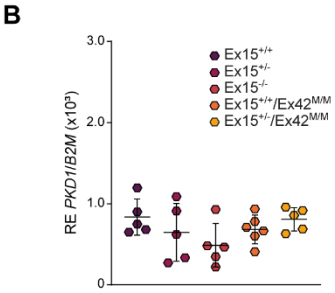
B
RE PKD1/B2M (x10³)
3.0
2.0
1.0
0
Ex15+/+
Ex15+/-
Ex15-/-
Ex15+/+/Ex42M/M
Ex15+/-/Ex42M/M

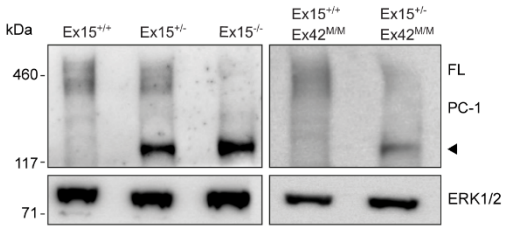
C
kDa
Ex15+/+
Ex15+/-
Ex15-/-
Ex15+/+ Ex42M/M
Ex15+/- Ex42M/M
460
117
71
FL
PC-1
ERK1/2

Figure 2

A

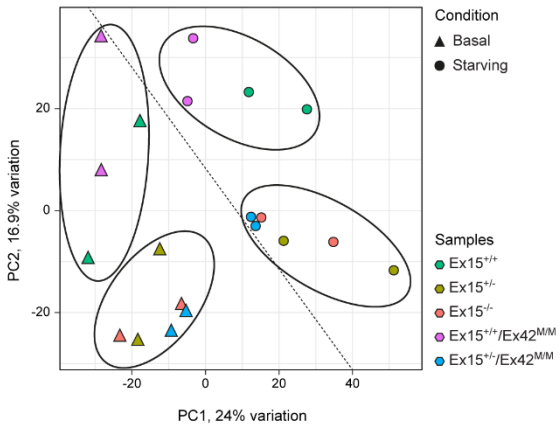
Condition
Basal
Starving
Samples
Ex15+/+
Ex15+/-
Ex15-/-
Ex15+/+/Ex42M/M
Ex15+/-/Ex42M/M
PC2, 16.9% variation
PC1, 24% variation
20
0
-20
-20
0
20
40

Figure 3

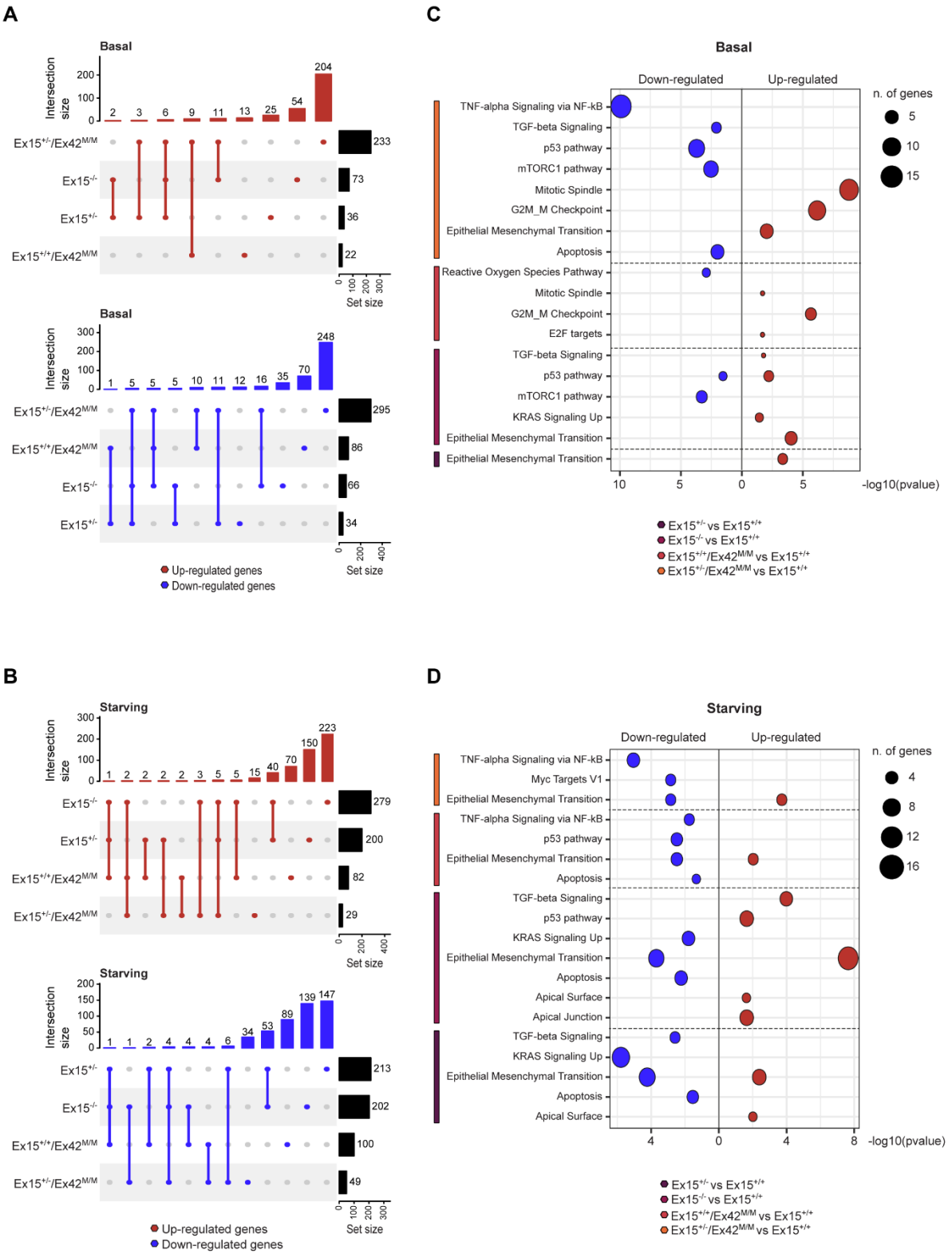
A
Basal
Intersection size
Ex15+/-/Ex42M/M
Ex15-/-
Ex15+/-
Ex15+/+/Ex42M/M
Set size
Basal
Up-regulated genes
Down-regulated genes
B
Starving
Starving
C
Basal
Down-regulated
Up-regulated
n. of genes
TNF-alpha Signaling via NF-kB
TGF-beta Signaling
p53 pathway
mTORC1 pathway
Mitotic Spindle
G2M_M Checkpoint
Epithelial Mesenchymal Transition
Apoptosis
Reactive Oxygen Species Pathway
E2F targets
KRAS Signaling Up
-log10(pvalue)
Ex15+/- vs Ex15+/+
Ex15-/- vs Ex15+/+
Ex15+/+/Ex42M/M vs Ex15+/+
Ex15+/-/Ex42M/M vs Ex15+/+
D
Starving
Myc Targets V1
Apical Surface
Apical Junction

Figure 4

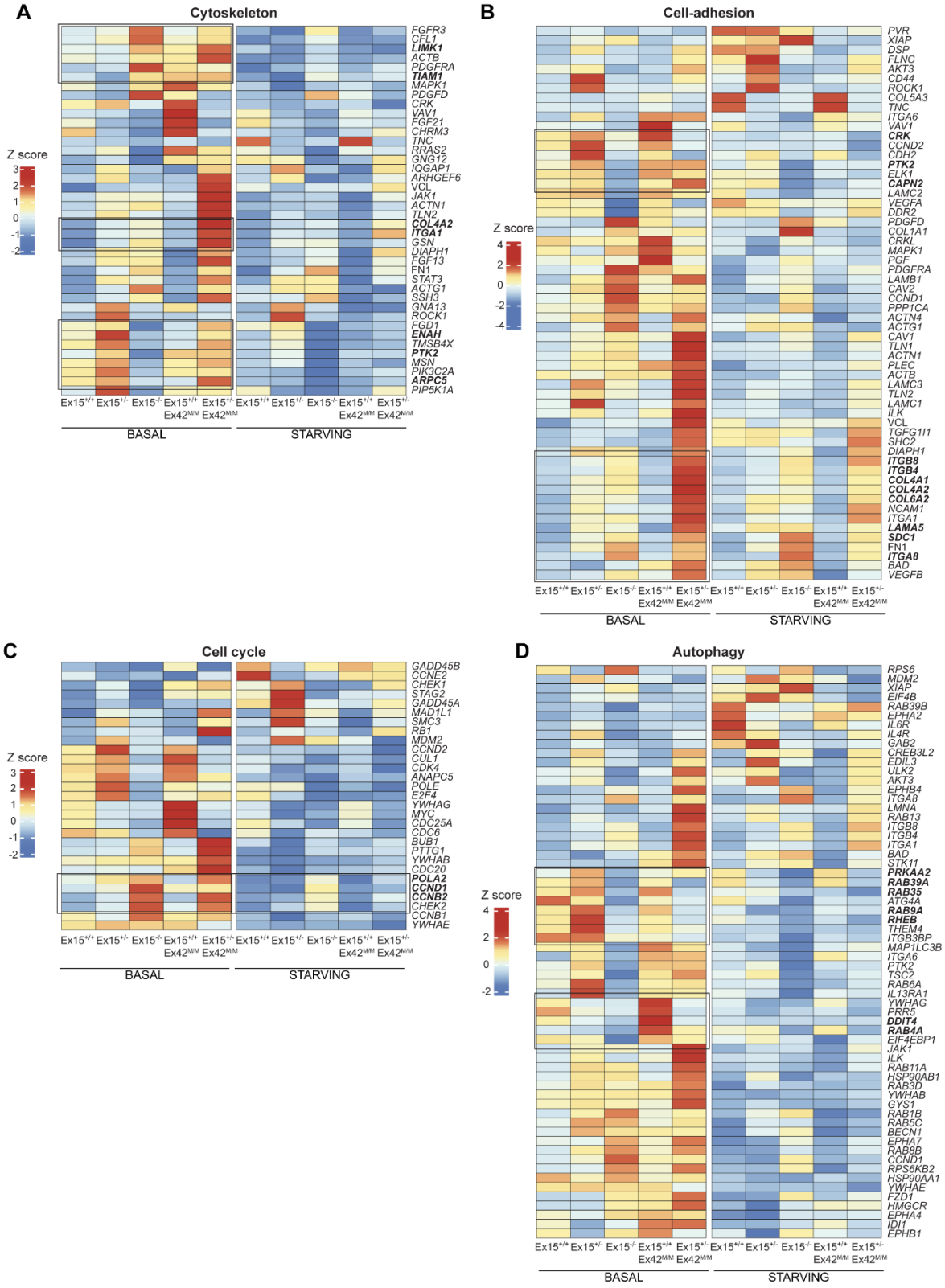
A
Cytoskeleton
Z score
3
2
1
0
-1
-2
FGFR3
CFL1
LIMK1
ACTB
PDGFRA
TIAM1
MAPK1
PDGFD
CRK
VAV1
FGF21
CHRM3
TNC
RRAS2
GNG12
IQGAP1
ARHGEF6
VCL
JAK1
ACTN1
TLN2
COL4A2
ITGA1
GSN
DIAPH1
FGF13
FN1
STAT3
ACTG1
SSH3
GNA13
ROCK1
FGD1
ENAH
TMSB4X
PTK2
MSN
PIK3C2A
ARPC5
PIP5K1A
Ex15+/+ Ex15+/- Ex15-/- Ex15+/+ Ex15+/- Ex15+/+ Ex15+/- Ex15-/- Ex15+/+ Ex15+/-
Ex42M/M Ex42M/M Ex42M/M Ex42M/M
BASAL
STARVING
B
Cell-adhesion
Z score
4
2
0
-2
-4
PVR
XIAP
DSP
FLNC
AKT3
CD44
ROCK1
COL5A3
TNC
ITGA6
VAV1
CRK
CCND2
CDH2
PTK2
ELK1
CAPN2
LAMC2
VEGFA
DDR2
PDGFD
COL1A1
CRKL
MAPK1
PGF
PDGFRA
LAMB1
CAV2
CCND1
PPP1CA
ACTN4
ACTG1
CAV1
TLN1
ACTN1
PLEC
ACTB
LAMC3
TLN2
LAMC1
ILK
VCL
TGFG1I1
SHC2
DIAPH1
ITGB8
ITGB4
COL4A1
COL4A2
COL6A2
NCAM1
ITGA1
LAMA5
SDC1
FN1
ITGA8
BAD
VEGFB
Ex15+/+ Ex15+/- Ex15-/- Ex15+/+ Ex15+/- Ex15+/+ Ex15+/- Ex15-/- Ex15+/+ Ex15+/-
Ex42M/M Ex42M/M Ex42M/M Ex42M/M
BASAL
STARVING
C
Cell cycle
Z score
3
2
1
0
-1
-2
GADD45B
CCNE2
CHEK1
STAG2
GADD45A
MAD1L1
SMC3
RB1
MDM2
CCND2
CUL1
CDK4
ANAPC5
POLE
E2F4
YWHAG
MYC
CDC25A
CDC6
BUB1
PTTG1
YWHAB
CDC20
POLA2
CCND1
CCNB2
CHEK2
CCNB1
YWHAE
Ex15+/+ Ex15+/- Ex15-/- Ex15+/+ Ex15+/- Ex15+/+ Ex15+/- Ex15-/- Ex15+/+ Ex15+/-
Ex42M/M Ex42M/M Ex42M/M Ex42M/M
BASAL
STARVING
D
Autophagy
Z score
4
2
0
-2
RPS6
MDM2
XIAP
EIF4B
RAB39B
EPHA2
IL6R
IL4R
GAB2
CREB3L2
EDIL3
ULK2
AKT3
EPHB4
ITGA8
LMNA
RAB13
ITGB8
ITGB4
ITGA1
BAD
STK11
PRKAA2
RAB39A
RAB35
ATG4A
RAB9A
RHEB
THEM4
ITGB3BP
MAP1LC3B
ITGA6
PTK2
TSC2
RAB6A
IL13RA1
YWHAG
PRR5
DDIT4
RAB4A
EIF4EBP1
JAK1
ILK
RAB11A
HSP90AB1
RAB3D
YWHAB
GYS1
RAB1B
RAB5C
BECN1
EPHA7
RAB8B
CCND1
RPS6KB2
HSP90AA1
YWHAE
FZD1
HMGCR
EPHA4
IDI1
EPHB1
Ex15+/+ Ex15+/- Ex15-/- Ex15+/+ Ex15+/- Ex15+/+ Ex15+/- Ex15-/- Ex15+/+ Ex15+/-
Ex42M/M Ex42M/M Ex42M/M Ex42M/M
BASAL
STARVING

Figure 5

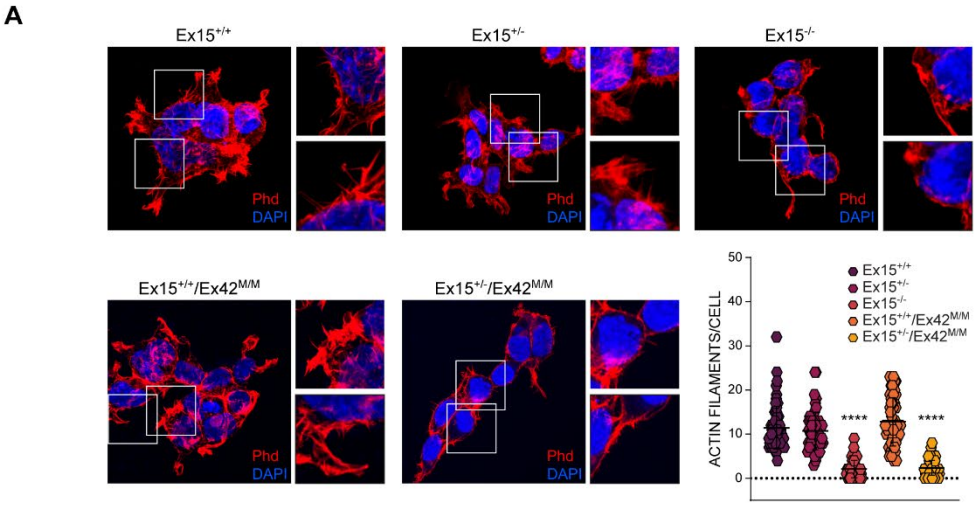
A
Ex15+/+
Ex15+/-
Ex15-/-
Phd
DAPI
Ex15+/+/Ex42M/M
Ex15+/-/Ex42M/M
ACTIN FILAMENTS/CELL
50
40
30
20
10
0
****
****

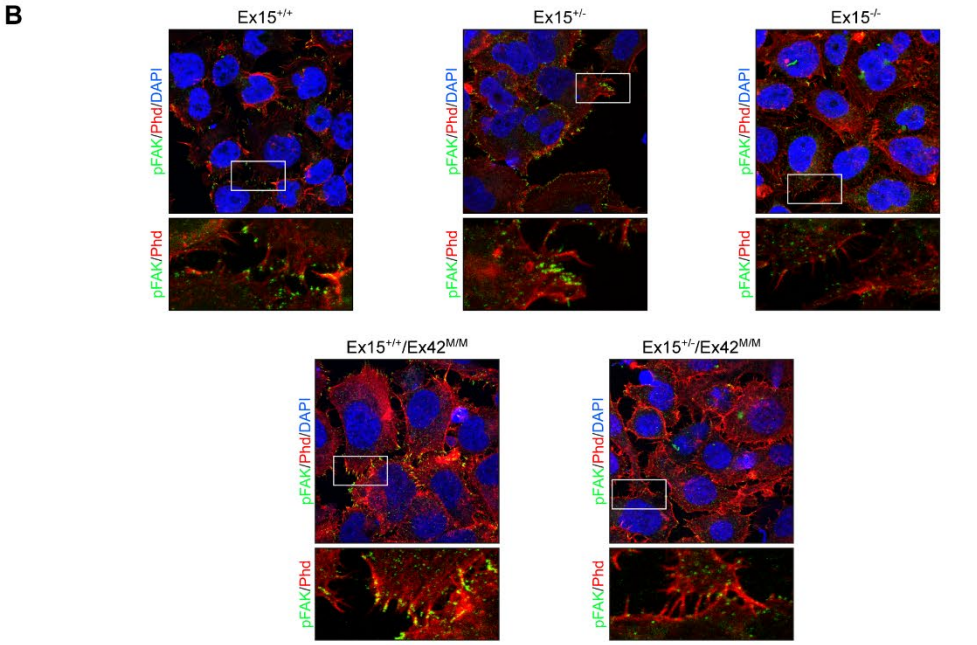
B
Ex15+/+
Ex15+/-
Ex15-/-
pFAK/Phd/DAPI
pFAK/Phd
Ex15+/+/Ex42M/M
Ex15+/-/Ex42M/M

Figure 6

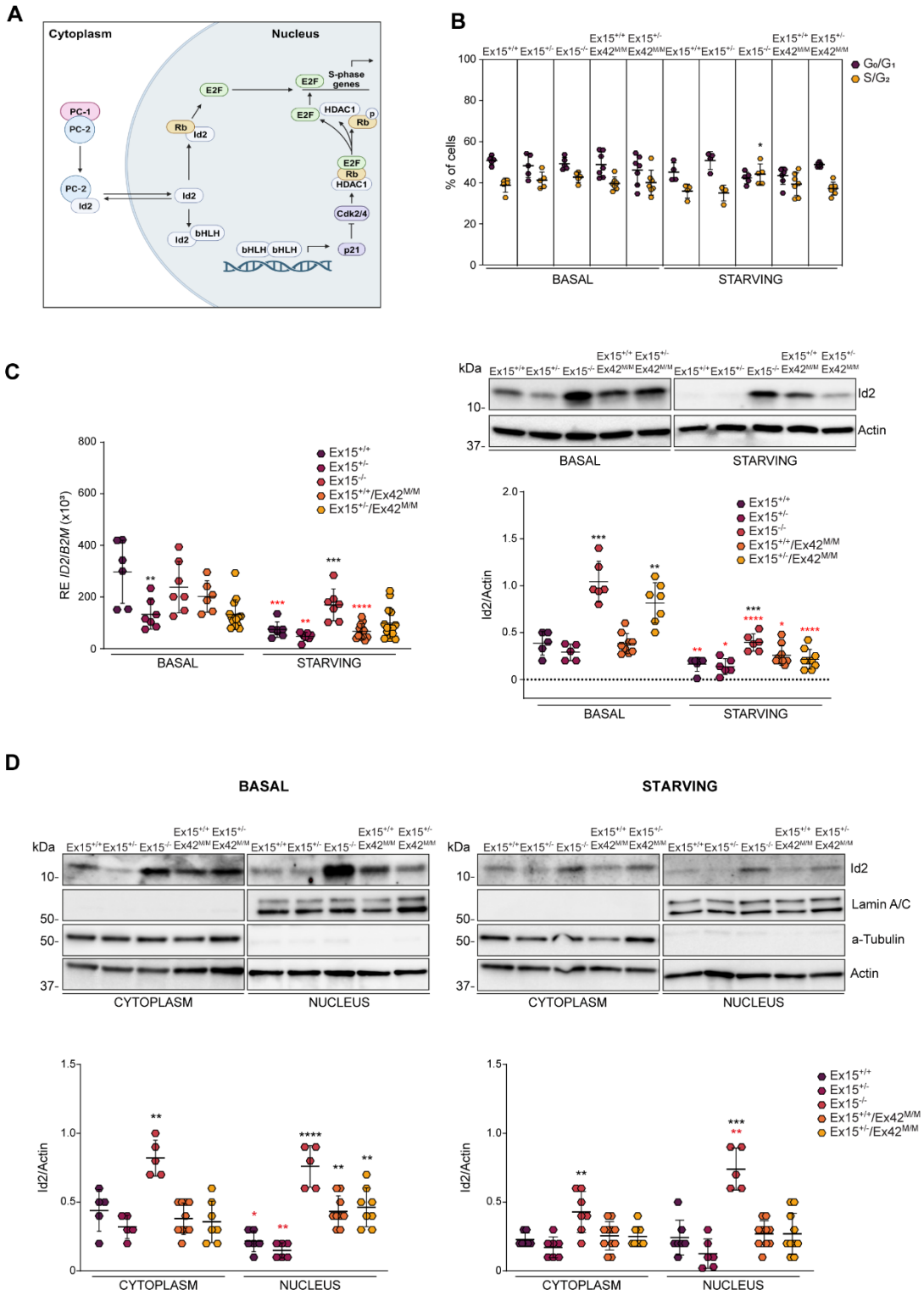
A
Cytoplasm
Nucleus
PC-1
PC-2
PC-2
Id2
Id2
bHLH
Id2
E2F
Rb
Id2
E2F
S-phase genes
E2F
HDAC1
p
Rb
E2F
Rb
HDAC1
Cdk2/4
bHLH bHLH
p21
B
% of cells
G0/G1
S/G2
BASAL
STARVING
C
RE ID2/B2M (x10³)
Ex15+/+
Ex15+/-
Ex15-/-
Ex15+/+/Ex42M/M
Ex15+/-/Ex42M/M
BASAL
STARVING
kDa
Id2
Actin
Id2/Actin
D
BASAL
STARVING
Id2
Lamin A/C
a-Tubulin
Actin
CYTOPLASM
NUCLEUS

Figure 7

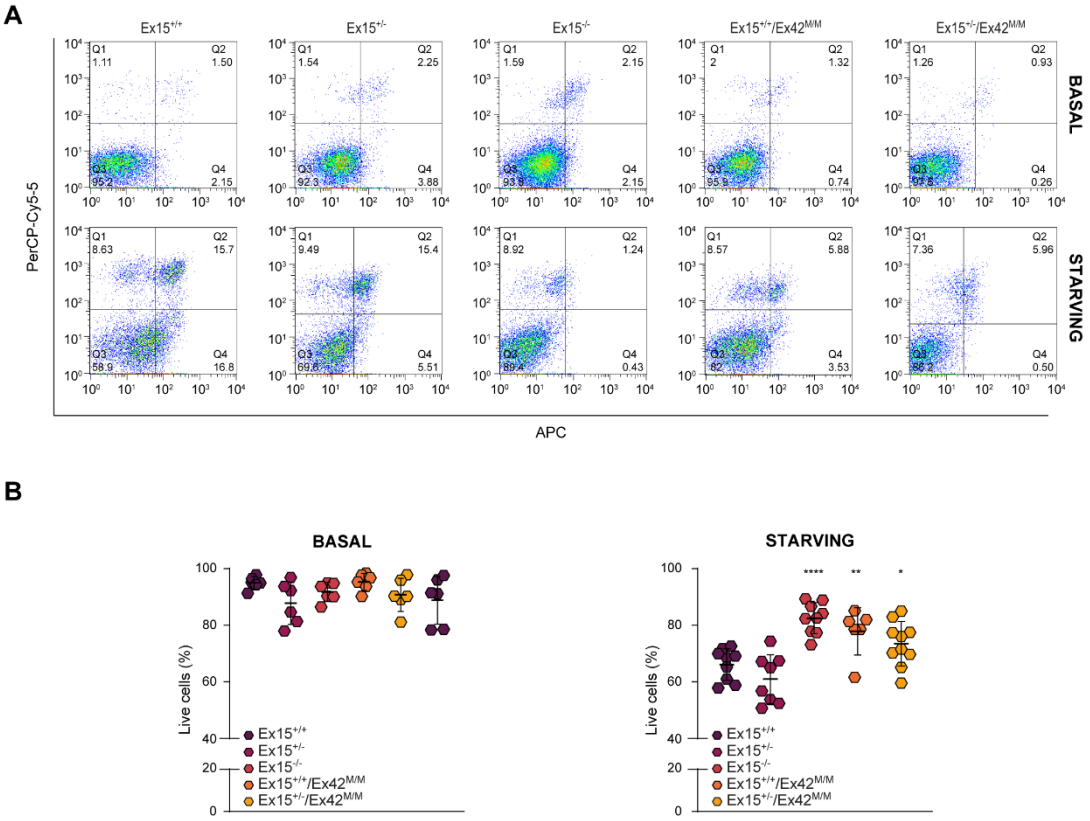
A
Ex15+/+
Ex15+/-
Ex15-/-
Ex15+/+/Ex42M/M
Ex15+/-/Ex42M/M
BASAL
STARVING
PerCP-Cy5-5
APC
B
BASAL
STARVING
Live cells (%)
Ex15+/+
Ex15+/-
Ex15-/-
Ex15+/+/Ex42M/M
Ex15+/-/Ex42M/M
****
**
*

Figure 8

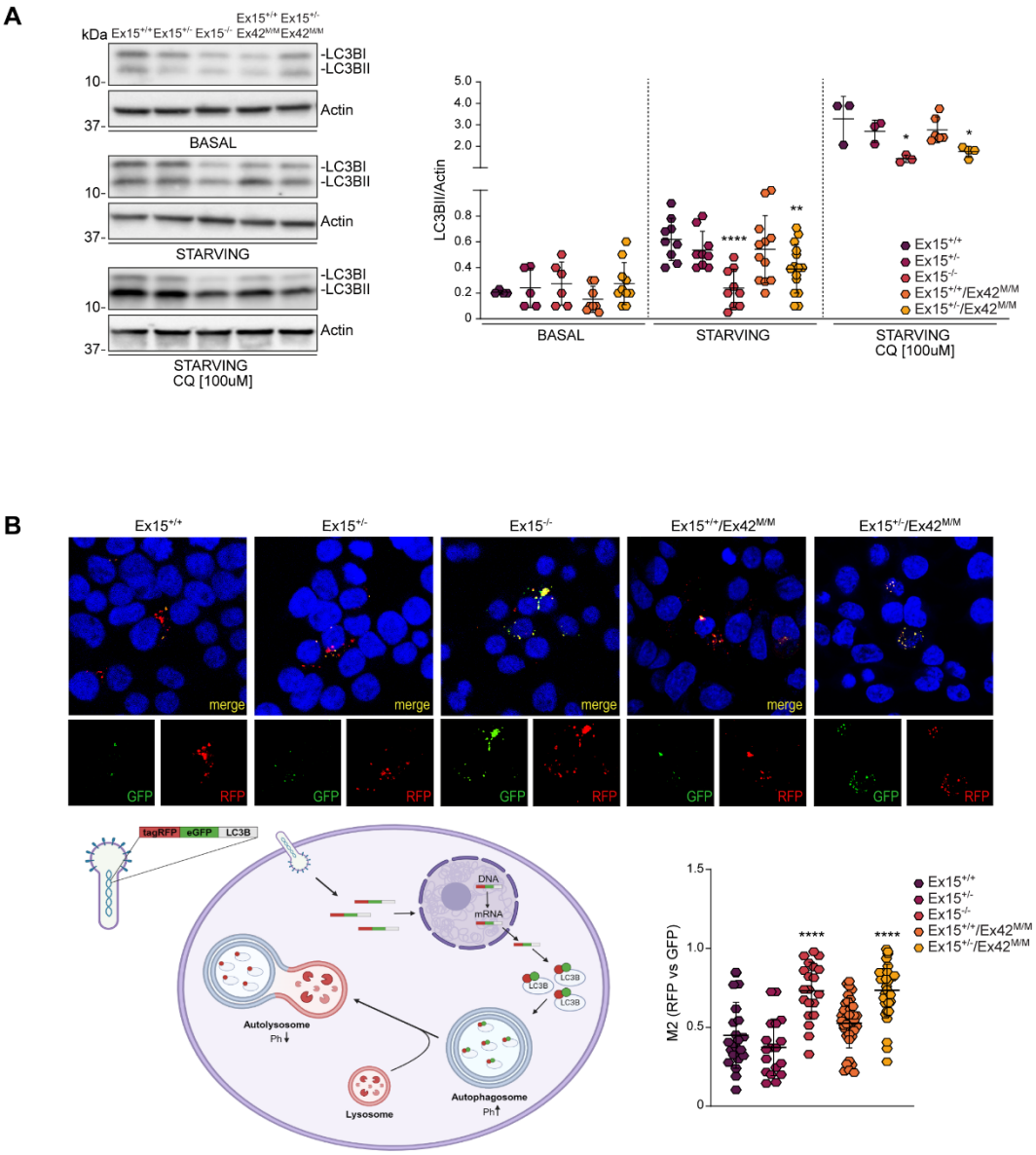
A
kDa Ex15+/+ Ex15+/- Ex15-/- Ex15+/+ Ex15+/- Ex42M/M Ex42M/M
-LC3BI
-LC3BII
10-
Actin
37-
BASAL
STARVING
STARVING
CQ [100uM]
LC3BII/Actin
5.0
4.0
3.0
2.0
0.8
0.6
0.4
0.2
0
****
**
*
Ex15+/+
Ex15+/-
Ex15-/-
Ex15+/+/Ex42M/M
Ex15+/-/Ex42M/M
BASAL
STARVING
STARVING
CQ [100uM]
B
Ex15+/+
Ex15+/-
Ex15-/-
Ex15+/+/Ex42M/M
Ex15+/-/Ex42M/M
merge
GFP
RFP
tagRFP
eGFP
LC3B
DNA
mRNA
LC3B
Autolysosome
Ph↓
Lysosome
Autophagosome
Ph↑
M2 (RFP vs GFP)
1.5
1.0
0.5
0
****
****
Ex15+/+
Ex15+/-
Ex15-/-
Ex15+/+/Ex42M/M
Ex15+/-/Ex42M/M

Figure 9